Chapter 5

Discussion

Methodical prerequisites to examine trabecular bone architecture

This study is based on high resolution CT images. Concerning the quantification and interpretation of trabecular architectures, two factors are crucial. The first factor is the **imaging quality**. With regard to some assumptions about allometric scaling of trabecular elements, correct images of the trabecular architecture are essential. Recent studies of Swartz et al. (1998), Fajardo & Müller (2001), and Fajardo et al. (2002) mentioned that trabecular thickness does not vary significantly between different species with different body sizes. Only Mullender et al. (1996) noted a slight decrease in trabecular thickness with decreasing body size. However, the statement about nearly homogeneous trabecular thicknesses regardless of body size contradicts the adaptation of bone density and structure to applied loads (Williams & Lewis 1982, Jensen et al. 1990). Due to adaptation, trabeculae will reach a thickness which is mechanically required. The formation of surplus bone mass would contradict the economic principle of bone, whereas inadequately small trabeculae would not be able to support bone properly. Due to the fact that body weight and size influences the stress magnitude in bone, different trabecular thicknesses between different sized species are to be expected.

The study of Swartz et al. (1998) concluded also that trabecular thickness does not vary between different anatomical regions in bone by using a rather oversimplified method. They used 2D pictures of the most distal lying proximal trabeculae of mammal humeri and femora. By visual inspection they assumed that the trabeculae do not change in size in epiphyseal direction. This seems unlikely as the loads are directed from the articular surface towards the shaft and by the same time the cancellous bone volume on which they act decreases and the ratio of load per cancellous bone volume increases. Therefore, the load magnitude on single trabeculae in sub-articular regions is expected to be lower, compared to the load magnitude of single trabeculae in distal parts, ignoring the influence of cortical bone. Thus different stress levels evolve along proximal bone, influencing composition and structure of trabeculae. Additionally, the measurements done by Swartz et al. (1998) did not take into account the spatial orientation of the trabeculae. Trabeculae running obliquely with respect to the imageing plane may occur

thicker than they actually are (WHITHOUSE & DYSON 1974). However, WHITHOUSE & DYSON stated in a scanning electron microscopy study of 1974, that trabecular diameter in human proximal femora can differ by more than a threefold between different regions. Such a substantial characteristic as spatial differences in trabecular thickness are expected to exist in all vertebrate long bones. Accurate 3D CT images can verify their existence.

Studies on trabecular thickness always rely on histomorphometric measurements. A 3D structure can not be accurately described by 2D images, as already mentioned by WHITHOUSE & DYSON (1974). The **formulae calculating the histomorphometric parameters** from 3D CT images build the second factor which is crucial for any interpretation. If a formula is based on mathematical geometric assumptions like, for example, the parallel plate model, it will give inaccurate results for mainly rod-like architectures, while a formula referring to the rod model would bear a source of error for prolate or plate-like trabeculae. This emphasizes the need of real 3D histomorphometry.

The real 3D histomorphometric evaluation of CT data, as the prime method, may be influenced by some factors, too. The resolution of the CT images and the chosen threshold to separate bone from fossil fillings, marrow or air are crucial for obtaining correct results. If the diameters of single, fine trabeculae are depicted with only a few pixels across due to resolution, the partial volume effect can hinder a correct evaluation of the trabecular thickness. The threshold to separate bone from other material should be defined individually for each 3D image, especially for fossil bone. The system setting as well as different kinds of fossilization influence this threshold. An inappropriate threshold can exclude parts of the bone substance from, or include non-bone material in the evaluation.

Allometric effects in locomotor loading

The body size influences the locomotor loading conditions, as outlined in chapter 1.1. With regard to the present sample of non-human primates, body size and weight were kept in a small range. It is assumed that under these conditions allometric effects may be ignored and results are obtained which are comparable. The described architectural differences should be caused mainly by the different modes of habitual locomotion which induce different loading conditions. Only the human specimens exceed the relative small range of body weight and size. However, humans had to be considered too as they are specialists in primate locomotion and because of the well-founded knowledge about their proximal femoral architecture, however, comparisons to the other species have to be drawn much more carefully.

External bone morphology

Each species possesses its distinct morphological characteristics, as described in chapter 4.1. It was shown that the external morphologic features vary slightly between the individuals but they are nonetheless consistent within a species. Therefore, it can be assumed that similar forces must

have acted on the femora of a sampled species, ignoring phylogenetic factors in a first estimation. The surface textures like on the greater trochanter for example are pronounced on male and bigger individuals. They are shaped through the forces transmitted by muscles, tendons, and ligaments inserting at these textures. As bigger individuals tend to have bigger muscle bodies, their muscle forces are higher compared to small individuals, giving rise to relatively pronounced textures on their femora.

The muscle insertions give further information about the way the forces are transmitted into the bone. In theory, the spatial orientation of prime muscles and their fibres should be reflected in the orientation of the cancellous bone architecture. In this study the focus was on trabecular architecture, therefore no investigation about muscle or tendon insertion on the femur was made. In future studies the connection between muscle strength, muscle insertion, and trabecular architecture can contribute to the knowledge of load directed adaptation of bone.

Cancellous bone architecture

As in external bone morphology, every species possesses its characteristic cancellous bone architecture. The accentuation of trajectories or fainter reinforcement structures varies between the individuals. Again, bigger individuals, which are mainly of male sex show these structures very well as compared to the smaller and female individuals. This goes along with the mean trabecular thickness (Tb.Th) which tends to be large in big individuals of a species while it is definitely smaller in small individuals (Table C.1). Further, there seems to be a relation between the shape of the trabeculae and the size of the individuals in *Papio hamadryas*, *Presbytis entellus*, and *Homo sapiens*. Bigger individuals have a higher amount of plate-like trabeculae while smaller individuals possess more rod-like or prolate trabeculae (Table C.1). In *Alouatta seniculus* and *Hylobates* no definite relation between trabecular shape and individual size is recognizable.

It was hypothesized in Scherf (2000) and Scherf et al. (2005) that plate-like trabeculae can transfer maximum loads from various directions in the plane of their extension while rod-like ones can transfer high loads only when they are loaded axially. This hypothesis is now being extended to include the influence of the size factor on trabecular shape. As big individuals exert higher loads on their femora than small individuals, the loads acting on similar sized trabeculae would be higher in bigger individuals than in smaller ones. An increase of bone mass by building plate-like trabeculae does not only adjust the bone mass to the loading condition but also incorporate an extra safety factor in permitting the transfer of loads from different directions in which loads are transmitted slightly more frequently. As the relation between size and trabecular shape was found only in those species, which practise a habitual hind limb load intensive locomotion, this safety factor might be compulsory there, compared to *Alouatta seniculus* and *Hylobates* which rarely apply high loads to their hind limbs.

Alouatta seniculus

The arrangement of cancellous bone characterizes the different loading conditions caused by

different kinds of locomotion. The relatively low loads subjected to the hind limbs of *Alouatta seniculus* during its preferred climbing locomotion are reflected by an open cancellous bone structure with two weak preferred directions of alignment in the region of the femoral head and neck. During climbing the loading direction varies in accordance to the position of the limb which adjusts to different substrates. The variability of limb postures is highest during climbing, compared to other kinds of locomotion, during which the thigh gets moved mainly in para-sagittal plains. Therefore, no definite trajectories evolve by predominate climbing movements. The high loading conditions occurring in jumping occur very rarely and thus do not cause an adjustment of cancellous bone, such as reinforcement structures or trajectories (see Chapter 1.1: Nature of loading conditions and other factors which influence bone).

Referring to the investigation of Grand (1968b) the Musculus glutaeus maximus, Musculus glutaeus minimus, and Musculus glutaeus medius, fused with the Musculus piriformes, insert at the greater trochanter of the howler monkey. The Musculus glutaeus maximus was identified as extensor, while Musculus glutaeus minimus, Musculus glutaeus medius and Musculus piriformes were described as abductors and rotators. All these muscles are being strained to a lesser extend during climbing as they do not need to generate high propulsive forces, as compared to a locomotion which involves frequent jumping and running. In accordance with the relative low loads acting on it, the greater trochanter of *Alouatta seniculus* is small and supported by relatively few trabeculae. The mainly plate-like trabeculae of the greater trochanter are lying perpendicular to the cortex. In the lesser trochanter the trabecular alignment of *Alouatta seniculus* changes from a median-sagittal direction anteriorly to a sub-transverse direction posteriorly. This seems to be a reflection of the different directions of action of the flexion muscles (Musculus psoas major, Grand 1968b) probably induced by climbing movements.

Presbytis entellus

The agile and rather load intensive locomotion of *Presbytis entellus* causes a denser and higher connected trabecular network compared to *Alouatta seniculus*. A strong trajectorial bundle runs from the lower part of the femoral neck through the femoral head to its proximal end. This trajectory transmits high loads which act directly on the femoral head. These loads occur during running and leaping, when the femoral head gets pressed into the acetabulum by muscles and body weight. The robust shape of the greater trochanter, its higher position in relation to the femoral head, and its complex cancellous bone structure are likely to be caused by high stresses brought about the muscles inserting in the greater trochanter. Among these muscles the extensor muscles generate the main propulsive force during running and jumping and climbing of vertical substrates (see Chapter 2.1.2). As a description of the trabecular architecture of the lesser trochanter was only obtainable from the most mature specimen, no reliable conclusion can be drawn. However, as the trabeculae in this specimen are all inclined laterally a strong flexor muscle force acting in one direction on the lesser trochanter must be assumed.

Papio hamadryas

Papio hamadryas can be characterized as quadrupedal, terrestrial primate. Especially the heavy males put high loads on their hind limbs while running. The trabecular architecture displayed by the 3D CT images shows a close network of relatively thick trabeculae in the superior part of the femoral head. This structure is somewhat similar to the "compressive trajectory" in *Homo sapiens* and can be interpreted in a similar way. In humans the main loads of bipedal locomotion act on the superior region of the femoral head across an angle of approximately 20°, corresponding to the "compressive trajectory". In comparison to bipedal walking the body of *Papio hamadryas* has not to be balanced on two limbs and it is possible to rotate the femoral head around a bigger angle during fast quadrupedal locomotion. In this way high loads are transmitted across a bigger area of the femoral head than during bipedal locomotion. Therefore, this close network might be a sign of the high loads caused during quadrupedal running. A similar feature was found in *Presbytis entellus*, but due to the juvenile age of the sampled individuals and the close distance to the epiphyseal split, its relation to locomotor loading is unclear.

The greater trochanter of *Papio hamadryas* is composed of a complex trabecular architecture and overtops the femoral head. It is comparable to the greater trochanter of *Presbytis entellus* and can be interpreted in a same way: the shape and the trabecular architecture are possibly reflections of strong forces caused by extensor muscles, contributing to the propulsive force during fast quadrupedal locomotion. The Musculus glutaeus medius, Musculus glutaeus minimus, and Musculus piriformis are inserting at the greater trochanter of *Papio leucophaeus* and are identified to perform extension, abduction, inward rotation, and outward rotation (Fischer 1961). A similar situation is assumed for *Papio hamadryas*. In the lesser trochanter of *Papio hamadryas* two directions of alignment can be noted. In the anterior half the trabeculae are inclined laterally while in the posterior-most region the trabeculae are aligned in a sub-transverse plain. Between these two areas a fine trabecular network without a definite direction of alignment is present. These different directions of alignment may be sings of different directions of action of the flexion muscles inserting in the lesser trochanter (Musculus iliopsoas, according to observations in *Papio leucophaeus*, Fischer 1961). The different gaits may be the reason for the change in the action of direction of the flexors in *Papio hamadryas*.

Hylobates syndactylus / lar moloch

The gibbons, *Hylobates syndactylus* and *Hylobates lar moloch*, have a dispersed trabecular bone architecture. The distribution of cancellous bone is nearly homogeneous. The main difference between the two gibbon species consists in the spatial density of the trabeculae. *Hylobates syndactylus* has a higher spatial density of trabeculae compared to *Hylobates lar moloch*. This could be due to the overall higher loads put on the femora of *Hylobates syndactylus* by its higher body weight. Both species show two sheaves of plate-like trabeculae, running from the femoral neck into the head. In *Hylobates syndactylus* the inferior sheaf crosses the femoral head and end at the cortex above the fovea capitis, while in the silvery gibbon both sheaves can only be

tracked to the middle of the femoral head. The accentuation of the inferior structure in *Hylobates syndactylus* is probably related to the increased practice of climbing, i.e. putting on frequent loads on the hind limbs, whereas *Hylobates lar moloch* climbs less frequently (see Chapter 2.1.4). The greater trochanter is quite small on all *Hylobates* specimens but definitely bigger compared to *Alouatta seniculus*. Its architecture resembles the architecture of the greater trochanter in *Papio hamadryas*. As the hind limbs are tucked up during brachiation, the abduction muscles inserting in the greater trochanter will experience stress often in *Hylobates*, probably causing a higher stress level compared to the climbing loads of *Alouatta seniculus*. However, this stress is certainly lower in the gibbon's greater trochanter compared to the baboons. Therefore, the greater trochanter of *Hylobates syndactylus / lar moloch* is definitely smaller compared to *Papio hamadryas*.

The cancellous bone network of the lesser trochanter shows different directions of alignment. In both gibbon species the trabeculae of the anterior half are inclined laterally, while in the posterior half *Hylobates lar moloch* shows an undirected network and in the *Hylobates syndactylus* specimens the trabeculae are reoriented and aligned in transverse direction. A similar change of alignment as in *Hylobates syndactylus* was found in *Alouatta seniculus*. It can be interpreted similarly to *Alouatta seniculus*, as a change of the direction of action of the flexion muscles inserting in the lesser trochanter. The differences between the muscles strained during climbing, walking, and tucking up the legs during brachiation of *Hylobates syndactylus* could cause such a change. *Hylobates lar moloch* climbs less and brachiates more, probably straining its flexor muscles in a rather uniform way which does not give rise to two directions of alignment in the lesser trochanter trabecular architecture. However, the sample size is too small, therefore the differences between the two gibbon species have to be interpreted carefully.

Homo sapiens

The gross arrangement of the cancellous bone in human femora is well known. The so called "compressive trajectory" and the "tensile trajectory" were identified in all specimens. Predominately compressive loads are transmitted through the compressive trajectory, caused by body weight and muscle forces, pulling the femoral head into the acetabulum. During this loading condition the femoral head and neck are acting like a lever and give rise to tensile strains, which are transmitted via the tensile trajectory. A third trajectory laterally-distally to the Ward's triangle was discernible, too. This latter trajectory is supposed to submit also predominantly tensile strains (VAN RIETBERGEN et al. 2003). These tensile strains are hypothesized to be caused by the pull of the abduction and extension muscles on the greater trochanter (Musculus glutaeus medius, Musculus glutaeus minimus, and Musculus piriformis, according to PLATZER et al. 1986). Abductors and extensors are important during bipedal locomotion and in order to stabilize the posture through the one legged stance phase. However, as bipedal locomotion consists mainly of walking, the loads caused by these muscles are steady but relatively low, while jumping and running cause much higher loads, up to multiples of the body weight. Therefore, as well as due to species specific postures the greater trochanter is much bigger at *Presbytis*

entellus and *Papio hamadryas* compared to the rather short and stout greater trochanter of *Homo sapiens*. The trabecular alignment of the lesser trochanter is similar to *Papio hamadryas*. In the anterior half the trabeculae are inclined slightly laterally and in the posterior half they begin to reorient. Finally they are aligned in transverse direction in the posterior-most part of the lesser trochanter. As outlined above, this change of the trabecular alignment may be caused by different loading directions of the flexion muscles (Musculus iliopsoas, PLATZER et al. 1986), due to different gaits.

Pliopithecus vindobonensis and Paidopithex rhenanus

The trabecular architectures of *Pliopithecus vindobonensis* and *Paidopithex rhenanus* are very similar. Therefore, the following descriptions and comparisons are true for both fossil species. They show a quite unique trabecular architecture which is in its overall appearance not comparable to one of the extant species, while some features are similar to the extant specimens. In the upper part of the femoral head a network of relatively thick and wide separated plate-like trabeculae is present, creating a cap-like structure. A similar arrangement was found in *Papio hamadryas* and *Presbytis entellus*. Concerning *Papio hamadryas* this structure was interpreted as a sign of high loading conditions, especially during quadrupedal running, while its origin in *Presbytis entellus* is unclear due to the juvenile age of the sampled individuals. The *Papio hamadryas* specimens were all of adult age, while for *Pliopithecus vindobonensis* and *Paidopithex rhenanus* no definite statement about their age is possible. The assumption of a rather adult age is supported by the fact that no epiphyseal split was found in the CT images, even so the teeth of individual I (O.E. 304 r) and II (1970/1397/22 r, 1970/1397/23 l) show a low wear state, probably indicating a sub-adult age. However, the biomechanical factors causing the described structure must have been the same in all specimens, if ontogenetic processes are excluded, indicating a frequent relative high loading of the femoral head in *Pliopithecus vindobonensis* and *Paidopithex rhenanus*, probably in connection with fast quadrupedal locomotion. Comparing the intensity of this feature in *Papio hamadryas* and the two fossil species, the loads acting on the fossil femora must have been less intensive in the two fossil species than in *Papio hamadryas*. Below the cap-like structure a dense network of thinner trabeculae is present in the fossil specimens. A similar feature was found only in *Hylobates lar moloch*, but the loading condition giving rise to this feature is unclear.

Two trajectories are present in the femoral head and neck region of the fossil species. The first trajectory runs from the proximal part of the inferior cortex of the femoral neck to the proximal end of the head. It crosses on its course the cap-like structure and the adjoining dense network of thin trabeculae which are described above. The second trajectory extends sub-parallel to the superior cortex of the neck and ends in the mid part of the femoral head at the dense network of thin trabeculae. The relative size of the greater trochanter is similar to *Hylobates*. In the superior half of the greater trochanter the trabecular architecture shows some features which are known from the other extant species and unique features in its inferior half. Therefore, it is not possible to infer the possible loading conditions of the greater trochanter in the fossil species directly

from the extant species. *Pliopithecus vindobonensis* has a prominent lesser trochanter, similar to *Papio hamadryas* but while the distal part is emphasized on *Papio hamadryas*, the lesser trochanter of *Pliopithecus vindobonensis* shows a rather homogenous shape. The trabeculae of the lesser trochanter are anteriorly inclined towards the lateral side, while posteriorly they align in transverse direction.

Referring to these observations it becomes obvious that the loading conditions of the proximal femur of *Pliopithecus vindobonensis* and *Paidopithex rhenanus* are different compared to *Alouatta seniculus* and *Hylobates* to which they have been compared previously, even so some similarities to *Hylobates* exist. Overall it seems that the trabecular architecture was able to transmit higher loads compared to those caused by brachiation or semibrachiation. The trajectories and the rather heterogeneous cancellous network in *Pliopithecus vindobonensis* and *Paidopithex rhenanus*, compared to the rather homogeneous cancellous network of *Alouatta seniculus* and *Hylobates* support this new hypothesis. The trabecular architecture of *Presbytis entellus* and *Homo sapiens* shows less similarities to *Pliopithecus vindobonensis* and *Paidopithex rhenanus*.

On the basis of these comparisons it is seems reasonable that *Pliopithecus vindobonensis* and *Paidopithex rhenanus* were rather locomotor generalists, occasionally performing some load intensive kinds of locomotion causing the relatively well aligned cancellous network and the structure of relatively thick trabeculae in the superior part of the femoral head. However, the gross architecture shows no signs for specialized, load intensive locomotion like in *Papio hamadryas* and *Presbytis entellus*, or even bipedal locomotion.

3D histomorphometry

It is hard to characterize locomotor preferences by just taking the trabecular architecture of the lesser trochanter into account. However, the quantification of the characteristics of the trabecular architecture yielded definite differences between the species (Table C.1), even though the described characteristics of the cancellous bone structure of the lesser trochanter were rather similar in all species (see Chapter 4.3.1). The diagrams of the size corrected parameters (Figures 4.48, 4.49, 4.50) show fixed relations between species with similar kinds of habitual locomotion. The relative position of the *Alouatta seniculus* and *Hylobates seniculus / lar moloch* data to each other remain the same. These species put rather low loads on their hind limbs during their habitual locomotion. The howler monkeys as well as the gibbons have a rather homogeneous trabecular architecture with just faint trajectories or directions of alignment which are believed to be a reflection of the low loading conditions of their femora.

Presbytis entellus and *Papio hamadryas* show a similar linkage in the relative position of their size corrected data. Both species practice rather load intensive kinds of locomotion by jumping and running frequently compared to the former species. They show a heterogeneously arranged gross cancellous bone structure, with definite trajectories and reinforcement structures in it, which are able to transmit high loads from definite directions. The *Homo sapiens* data

show no definite relation to one of the other species. This may be caused by the extreme size differences between *Homo sapiens* and the rest of this sample, indicating that the size correction by the 'bone volume fraction' (BV/TV) might be not sufficient for big size differences.

The position of the size corrected data of *Pliopithecus vindobonensis* and *Presbytis entellus* always retain a fixed relation to each other, displayed in the diagrams in figures 4.48, 4.49 and 4.50. This corresponds with the described characteristics of the trabecular architectures of *Pliopithecus vindobonensis*, indicating by its heterogeneity an all-round locomotor habit. However, regarding *Paidopithex rhenanus* only a weak relationship with *Pliopithecus vindobonensis* can be spotted and both fossil species are positioned far away from each other, despite their similarities in trabecular architecture. Therefore a similar clue as for *Pliopithecus vindobonensis* is difficult to obtain. A possible reason for the extreme positions of *Paidopithex rhenanus* and *Pliopithecus vindobonensis* could be founded in the different sample sizes of five *Pliopithecus vindobonensis* femora and just one *Paidopithex rhenanus* femur, or differences in the loading condition of the lesser trochanter. This discrepancy is an interesting question for future research.

Results of the FEM pilot study

The results of the FE modelling showed the influence of data reduction on FE analyses. For optimal results only original high resolution data should be used. Thus fine structures could be considered in the analyses, while conventional reduction techniques like the data skipping method used in this study deletes voxels of a data set. Depending on the trabecular architecture, voxel skipping can bring different results. A network of few and relatively thick trabeculae would be influenced just slightly by a simple skipping operation as elements with several voxel diameters will still stay intact after skipping of every other voxel. Only after several skipping steps trabecular connections will be deleted. A network of thin trabeculae with only two or three voxel diameters will get damaged even by a simple skipping, considering every other voxel. Concerning the structural variability in a specimen some parts can get damaged by voxel skipping more seriously than other parts.

However, each incomplete trabecular network which is transformed into a FE mesh will bring inaccurate results about the stress distribution in cancellous bone, due to the fact that structural elements are missing. The stress curves obtained in the preliminary study (Figures 4.53, 4.54) vary strongly between the two skipping levels, indicating structural differences caused by voxel skipping. With respect to the results of the test cubes no reliable conclusions can be drawn, too (Figures 4.55, 4.56, 4.57, 4.58). Therefore no FE analysis of the main sample was conducted.

Since it is inevitable to reduce data to enable FE modelling, specialized reduction techniques are of need. The combination of two voxels into one voxel and taking their individual grey values into account could be a helpful reduction method. However, fine elements could get deleted or increased in size by this method, if the threshold settings defining material versus non-material are chosen inappropriately. Additionally, this method is only advisable for a small number of

reduction steps as the error increases with each step. A structure sensitive reduction technique, distinguishing large bone volumes from fine structures would be most suitable. While a coarse FE mesh could be generated for large bone volumes, fine structures could be meshed by the single voxels of the original high resolution data set.

Chapter 6

Conclusion

High resolution computed tomography is an optimal tool to investigate cancellous bone structure of long bones. As a non-destructive method it is most appropriate as the specimen stays intact and can be subjected to further investigation. The high resolution CT images reveal that different locomotor habits cause different cancellous bone architectures in the proximal femur, which can be defined by their characteristic features. Two types in gross architecture can be distinguished. A homogeneous type, with a less directed trabecular network, as presented by *Alouatta seniculus* and *Hylobates seniculus / lar moloch*, and a heterogeneous type with a well directed trabecular network, as in *Homo sapiens*, *Presbytis entellus*, and *Papio hamadryas*. The homogeneous type goes along with low loading conditions acting on the hind limbs from various directions, as they occur during climbing. The heterogeneous type is associated with specialized types of locomotion, subjecting relative high loads on the hind limbs.

All species examined show some similarities in the gross structure of the cancellous bone of the lesser trochanter region. Nonetheless, definite differences exist between the species. These differences are quantified by histomorphometric analyses. The data of *Tb.Th**, *Tb.Sp** and *Tb.N** each plotted against *Conn.Dens** of the lesser trochanter region show a relationship to the formerly observed gross types of proximal femoral trabecular architecture (Figures 4.48, 4.49, 4.50). The data of those species with a rather homogeneous cancellous bone network (*Alouatta seniculus*, *Hylobates*) always retain a fixed relation to each other, while those species with a rather well structured, heterogeneous cancellous bone network (*Presbytis entellus*, *Papio hamadryas*) also retain a fixed relation, indicating a reflection of gross architectonically features even in definite regions of the whole bone.

The femora of *Paidopithex rhenanus* and *Pliopithecus vindobonensis* indicate, by their proximal trabecular architecture that both species have practiced a similar kind of locomotion, despite their differences in geological age and also slightly in size. As non of the extant species mirrors the characteristics of cancellous bone in the two fossil species, no direct inference about their locomotional preferences is possible. However, by comparing single architectonic features and results obtained for *Paidopithex rhenanus* and *Pliopithecus vindobonensis* to the extant species,

it can be concluded that both fossil species were locomotor generalists, habitually practising more load intensive locomotion as compared to *Alouatta seniculus* and *Hylobates*.

The present study yields new insight into the complex relation of locomotor loading and bone structure and forms a new basis for investigating cancellous bone architecture. A future combination of the high resolution CT analysis with other fields of study comprising research on locomotor behavior, muscular system, muscle insertions, composition of bone on micron level, and FEM studies, under the prerequisites defined in this study, will contribute to the knowledge of locomotor biomechanics and the generation of comprehensive models for different modes of habitual locomotion. Locomotion models of extant species developed on the basis of such combined approaches form the basis for locomotor interpretations of fossil species.

Appendix A

Specimen pictures

A.1 Extant Species

A.1.1 *Alouatta seniculus*

Figure A.1: Left femur of *Alouatta seniculus* (25 544 l) ♀, ventral view

Figure A.2: Left femur of *Alouatta seniculus* (25 544 l) ♀, dorsal view

Figure A.3: Left femur of *Alouatta seniculus* (25 545 l) ♀, ventral view

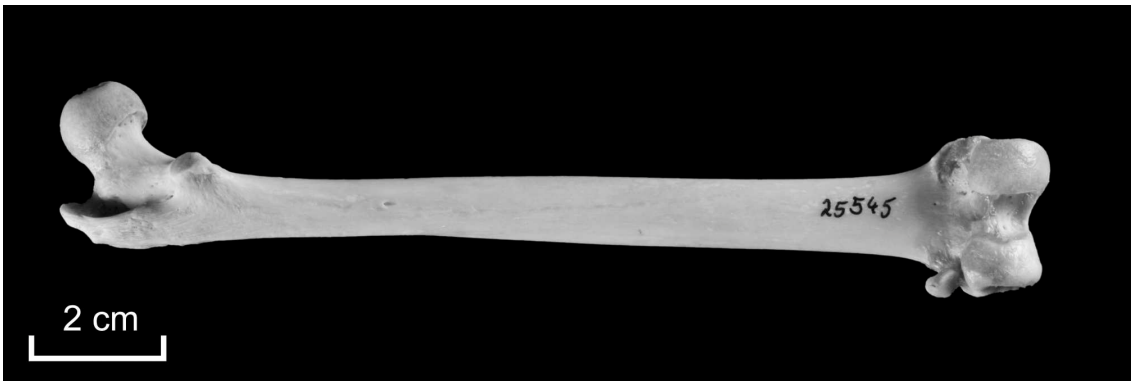

Figure A.4: Left femur of *Alouatta seniculus* (25 545 l) ♀, dorsal view

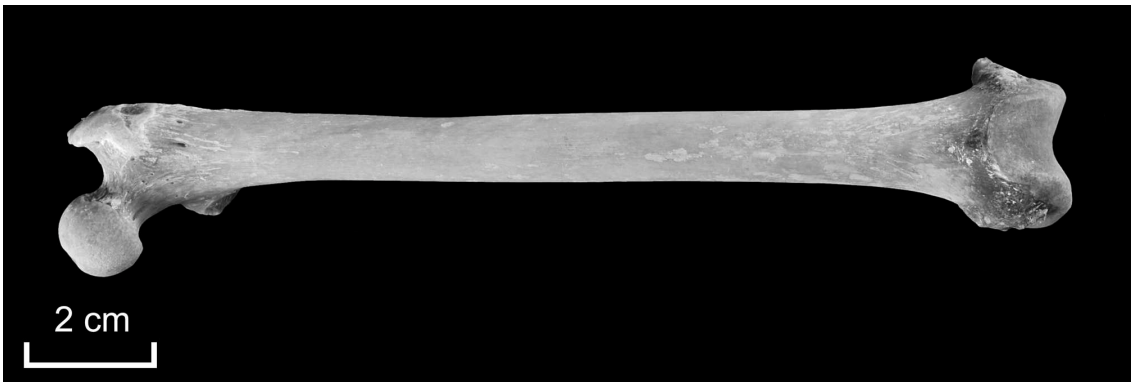

Figure A.5: Left femur of *Alouatta seniculus* (69.19 l) ♂, ventral view

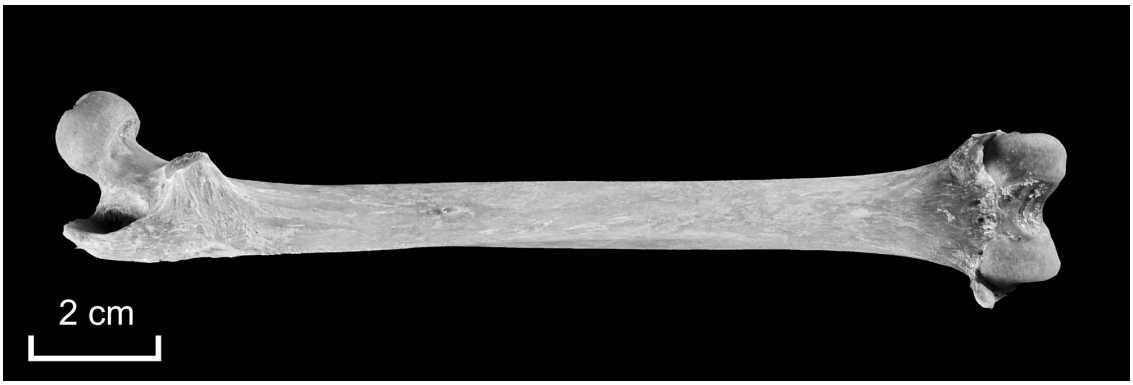

Figure A.6: Left femur of *Alouatta seniculus* (69.19 l) ♂, dorsal view

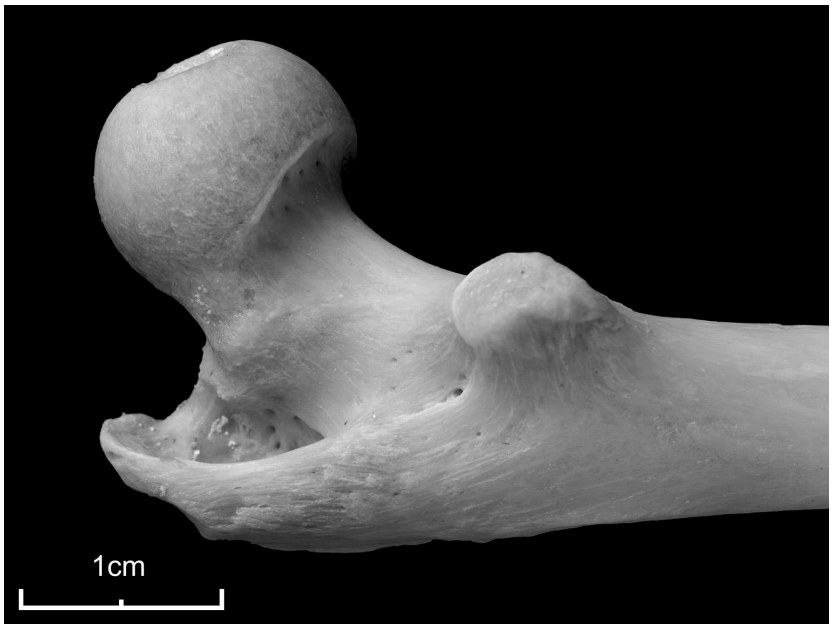

Figure A.7: Tuberculum next to the fossa trochanterica on *Alouatta seniculus* (25 544 l) ♀, dorsal view

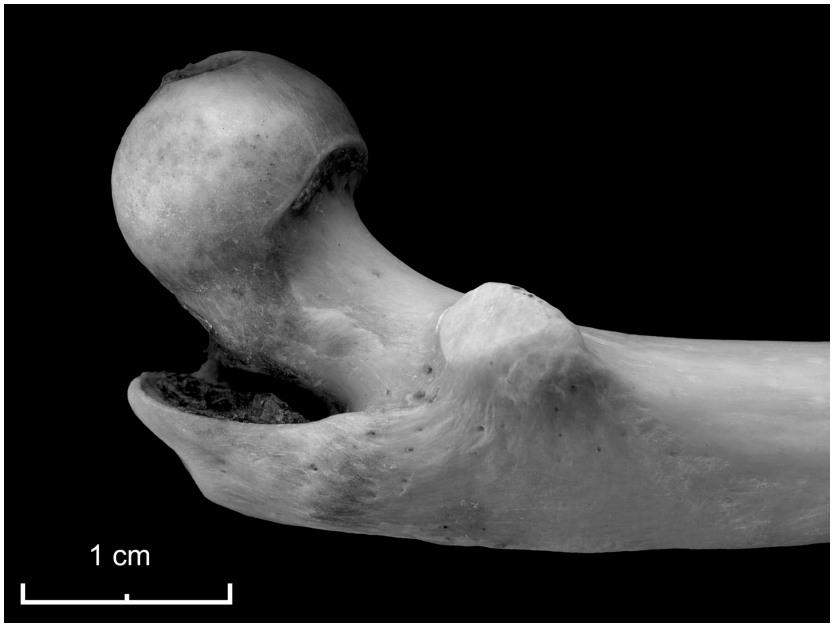

Figure A.8: Tuberculum next to the fossa trochanterica on *Alouatta seniculus* (25 544 l) ♀, dorsal view

A.1.2 *Presbytis entellus*

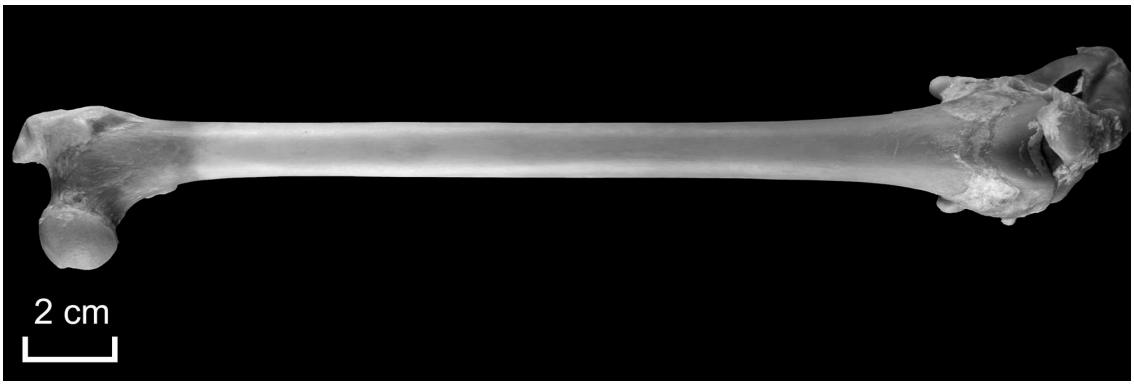

Figure A.9: Left femur of *Presbytis entellus* (4743 l), ventral view

Figure A.10: Left femur of *Presbytis entellus* (4743 l), dorsal view

Figure A.11: Left femur of *Presbytis entellus* (4745 l), ventral view

Figure A.12: Left femur of *Presbytis entellus* (4745 l), dorsal view

Figure A.13: Left femur of *Presbytis entellus* (4746 l), ventral view

Figure A.14: Left femur of *Presbytis entellus* (4746 l), dorsal view

Figure A.15: Left femur of *Presbytis entellus* (4734 l), ventral view

Figure A.16: Left femur of *Presbytis entellus* (4734 l), dorsal view

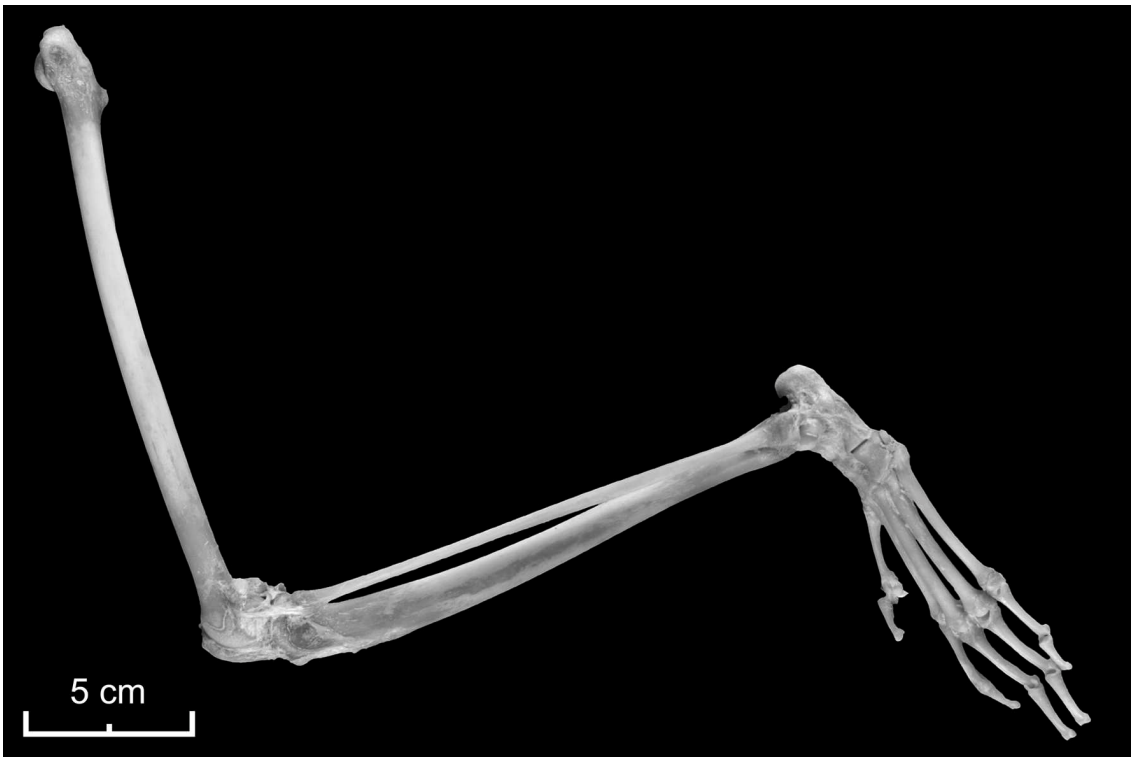

Figure A.17: Complete specimen of *Presbytis entellus* (4746 l), lateral view

A.1.3 *Papio hamadryas*

Figure A.18: Left femur of *Papio hamadryas* (1.553 l) ♀, ventral view

Figure A.19: Left femur of *Papio hamadryas* (1.553 l) ♀, dorsal view

Figure A.20: Left femur of *Papio hamadryas* (Ha VIII 83 l) ♂, ventral view

Figure A.21: Left femur of *Papio hamadryas* (Ha VIII 83 l) ♂, dorsal view

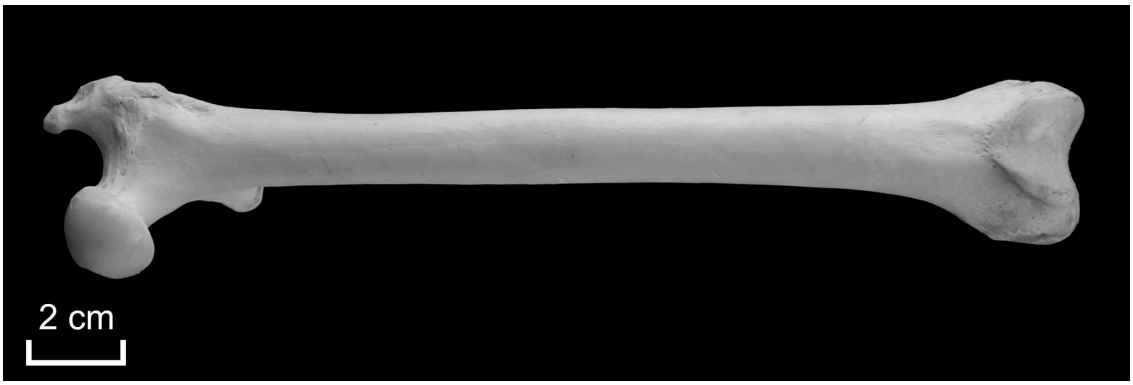

Figure A.22: Left femur of *Papio hamadryas* (Ha VIII 3 l) ♂, ventral view

Figure A.23: Left femur of *Papio hamadryas* (Ha VIII 3 l) ♂, dorsal view

Figure A.24: Left femur of *Papio hamadryas* (3212 l) ♂, ventral view

Figure A.25: Left femur of *Papio hamadryas* (3212 l) ♂, dorsal view

Figure A.26: Tuberculum next to the fossa trochanterica on *Papio hamadryas* (3212 l) ♂, dorsal view

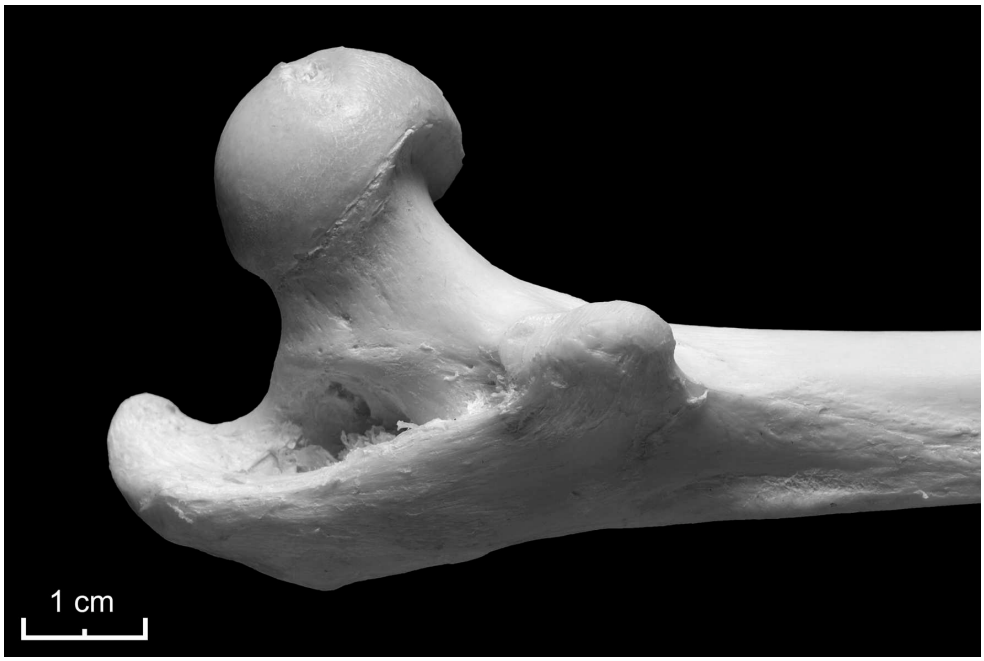

Figure A.27: Tuberculum next to the fossa trochanterica on *Papio hamadryas* (Ha VIII 83 l) ♂, dorsal view

Figure A.28: Tuberculum next to the fossa trochanterica on *Papio hamadryas* (Ha VIII 3 l) ♂, dorsal view

Figure A.29: Trochanter major on *Papio hamadryas* (3212 l) ♂, lateral view

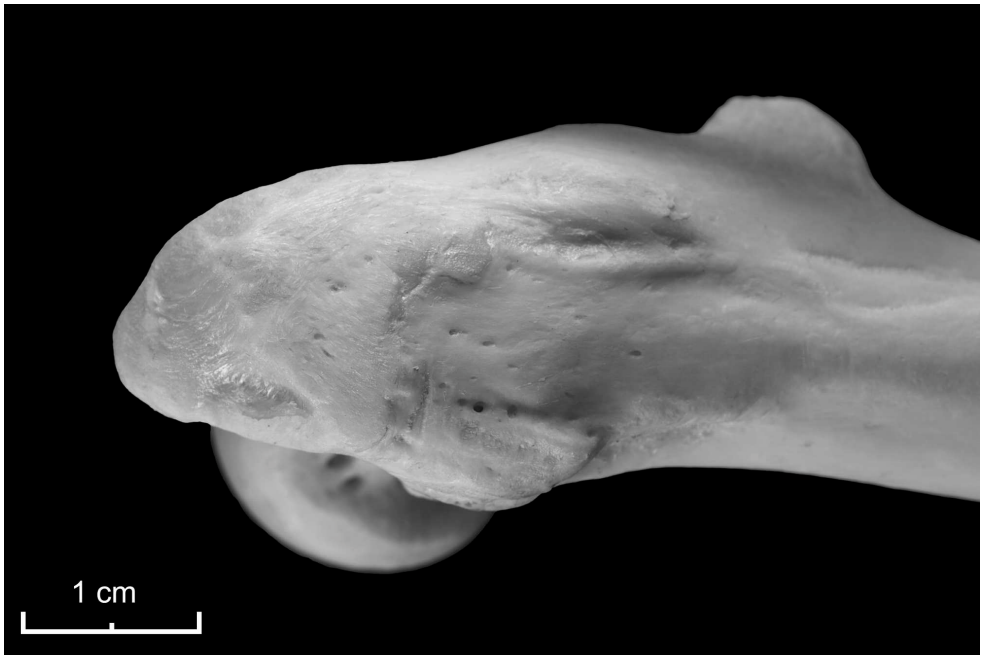

Figure A.30: Trochanter major on *Papio hamadryas* (Ha VIII 3 l) ♂, lateral view

A.1.4 *Hylobates seniculus / lar moloch*

Figure A.31: Left femur of *Hylobates seniculus* (6983 l) ♂, ventral view

Figure A.32: Left femur of *Hylobates seniculus* (6983 l) ♂, dorsal view

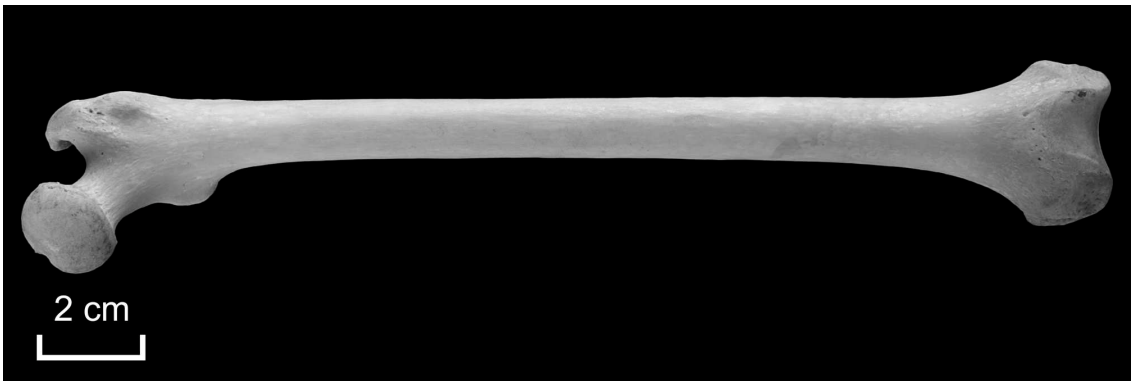

Figure A.33: Left femur of *Hylobates seniculus* (52.36. l) ♀, ventral view

Figure A.34: Left femur of *Hylobates seniculus* (52.36. l) ♀, dorsal view

Figure A.35: Right femur of *Hylobates lar moloch* (47 979 r) ♂, ventral view

Figure A.36: Right femur of *Hylobates lar moloch* (47 979 r) ♂, dorsal view

Figure A.37: Tuberculum on the posterior side of the femoral neck on *Hylobates lar moloch* (47 979 r) ♂

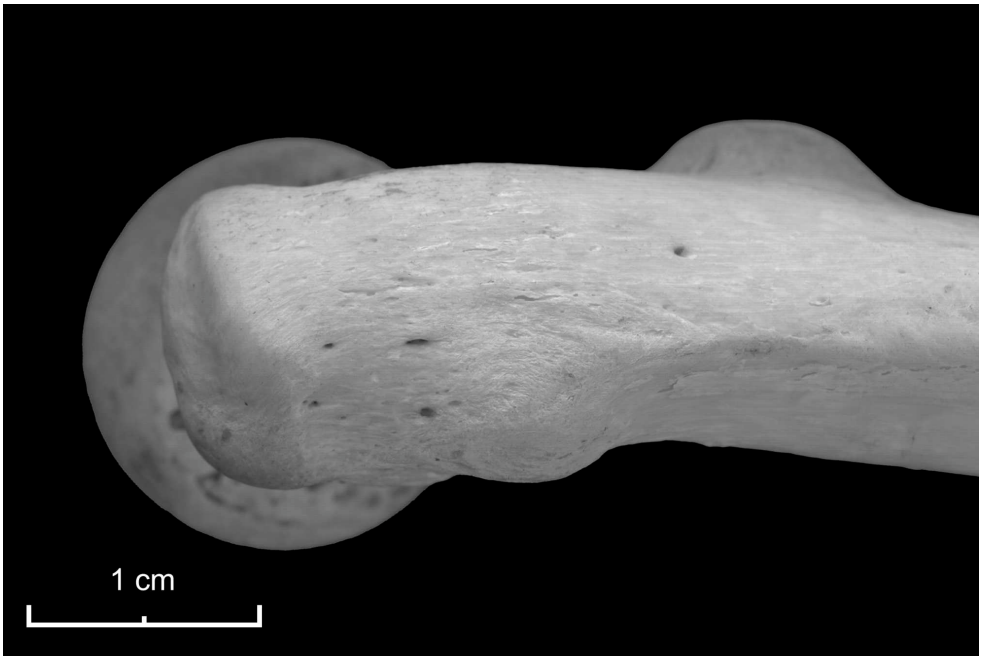

Figure A.38: Trochanter major with an anterior protuberance and the concave area at the superior tip on *Hylobates seniculus* (52.36. l) ♀

A.1.5 *Homo sapiens*

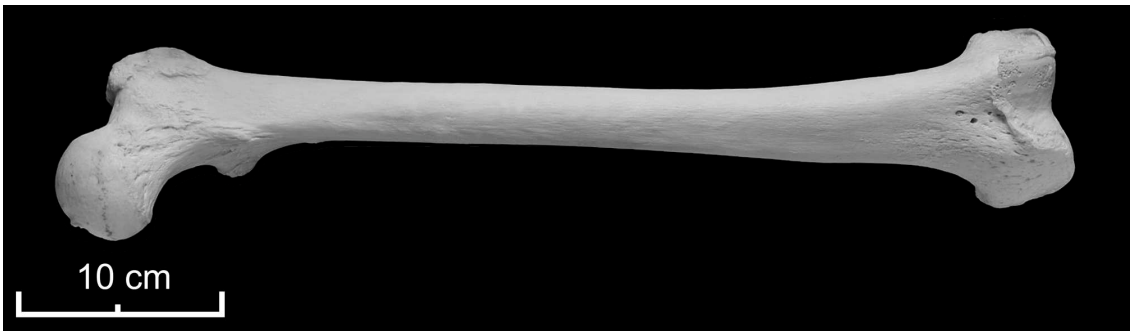

Figure A.39: Left femur of *Homo sapiens* (11 l) ♂, ventral view

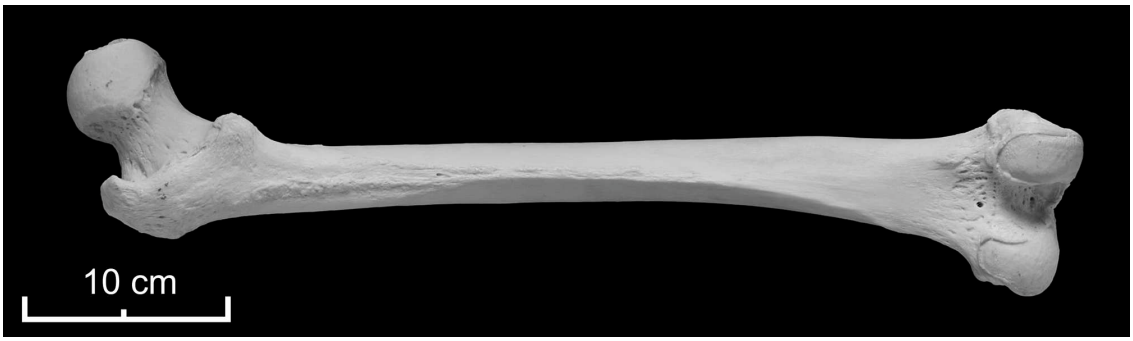

Figure A.40: Left femur of *Homo sapiens* (11 l) ♂, dorsal view

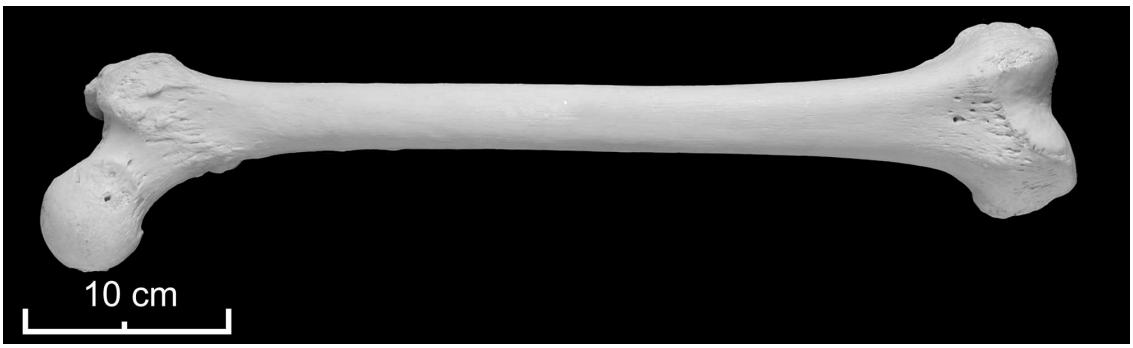

Figure A.41: Left femur of *Homo sapiens* (21 l) ♂, ventral view

Figure A.42: Left femur of *Homo sapiens* (21 l) ♂, dorsal view

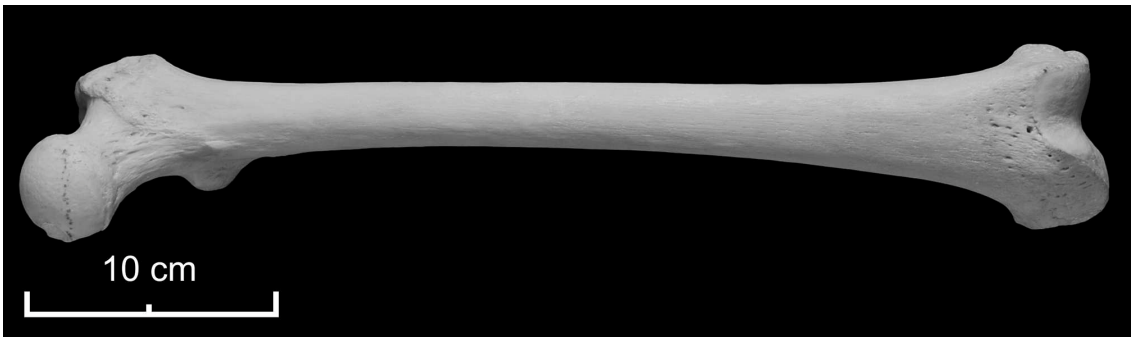

Figure A.43: Left femur of *Homo sapiens* (10 l) ♀, ventral view

Figure A.44: Left femur of *Homo sapiens* (10 l) ♀, dorsal view

Figure A.45: Left femur of *Homo sapiens* (22 l) ♀, ventral view

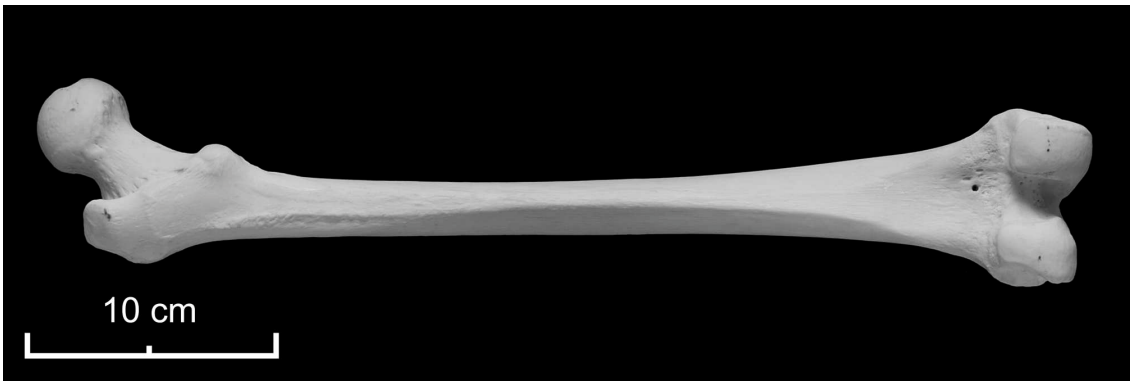

Figure A.46: Left femur of *Homo sapiens* (22 l) ♀, dorsal view

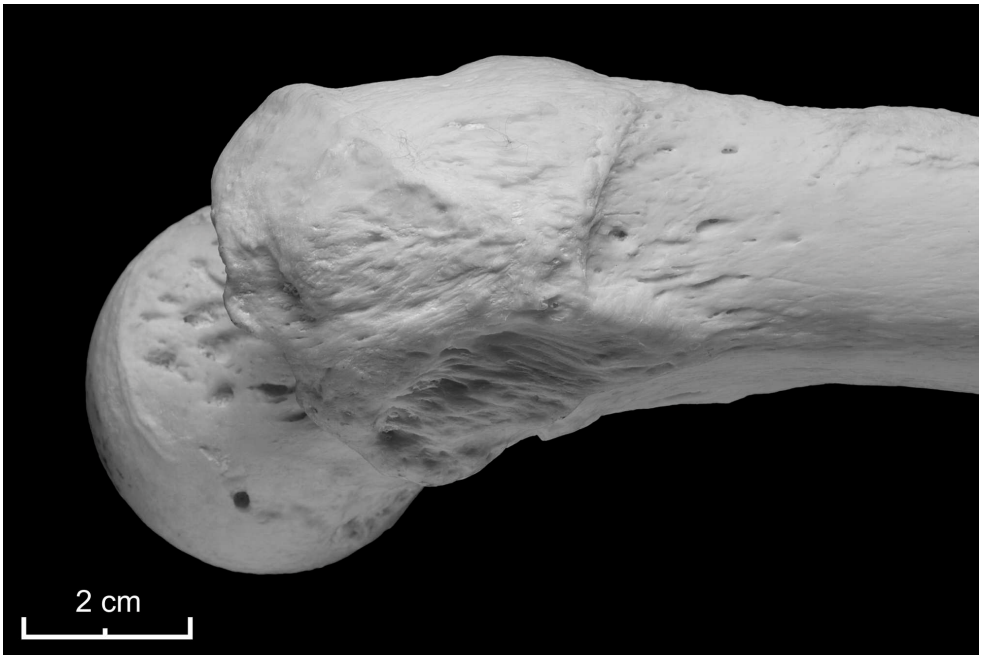

Figure A.47: Trochanter major on *Homo sapiens* (21 l) ♂, lateral view

A.2 Fossil Species

A.2.1 *Pliopithecus vindobonensis*

Figure A.48: Right femur of individuum I *Pliopithecus vindobonensis* (O.E. 304), ventral view

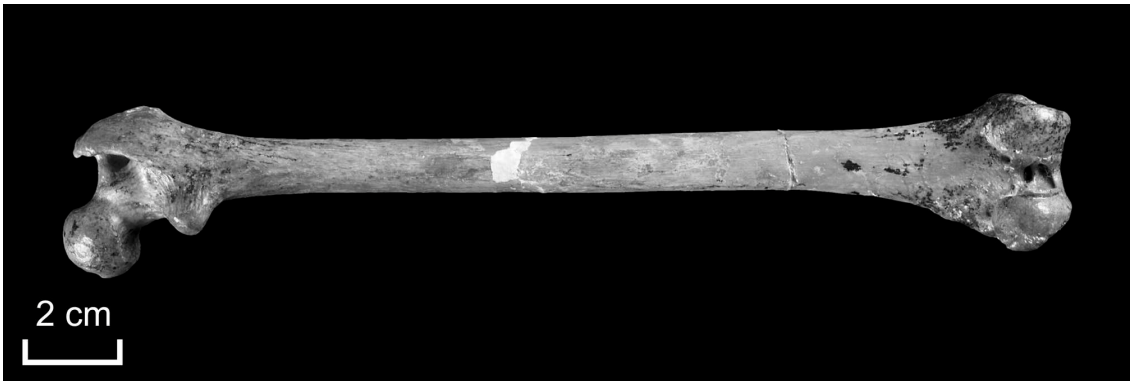

Figure A.49: Right femur of individuum I *Pliopithecus vindobonensis* (O.E. 304), dorsal view

Figure A.50: Left femur fragment of *Pliopithecus vindobonensis* (O.E. 559), ventral view

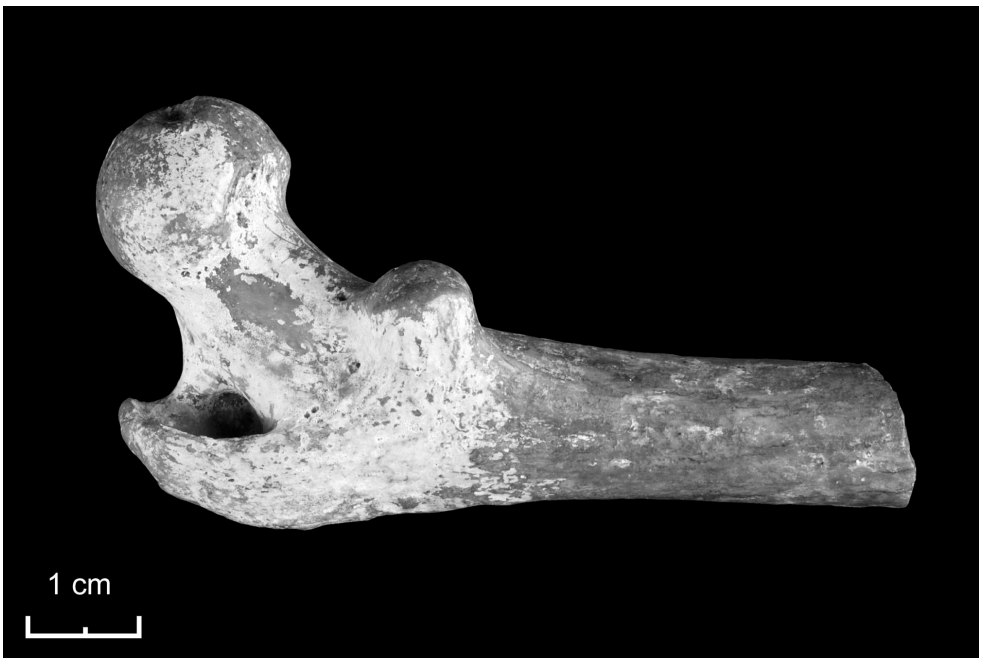

Figure A.51: Left femur fragment of *Pliopithecus vindobonensis* (O.E. 559), dorsal view

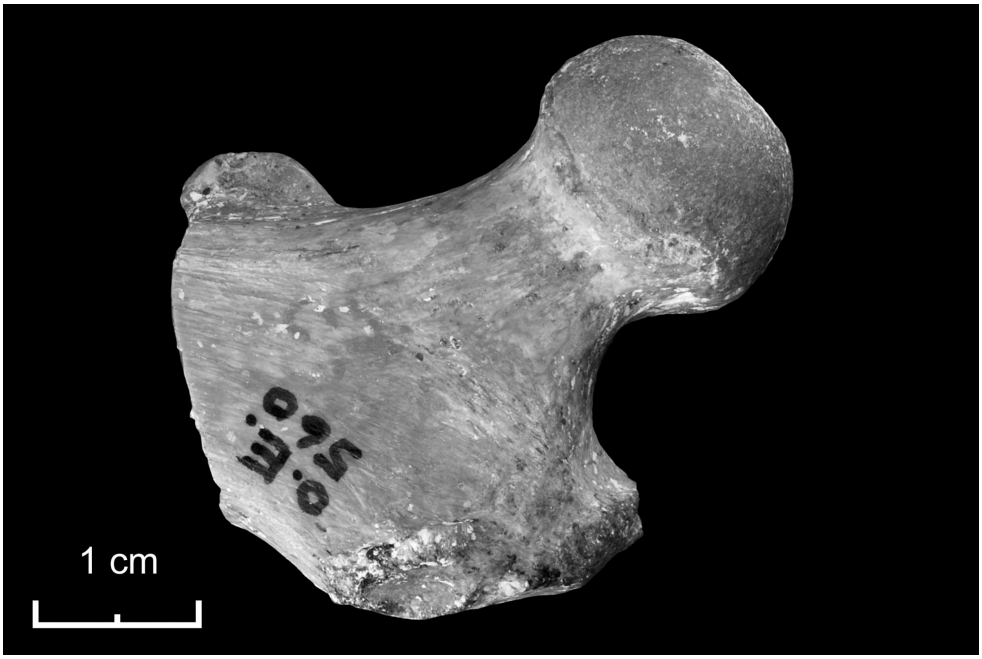

Figure A.52: Left femur fragment of *Pliopithecus vindobonensis* (O.E. 560), ventral view

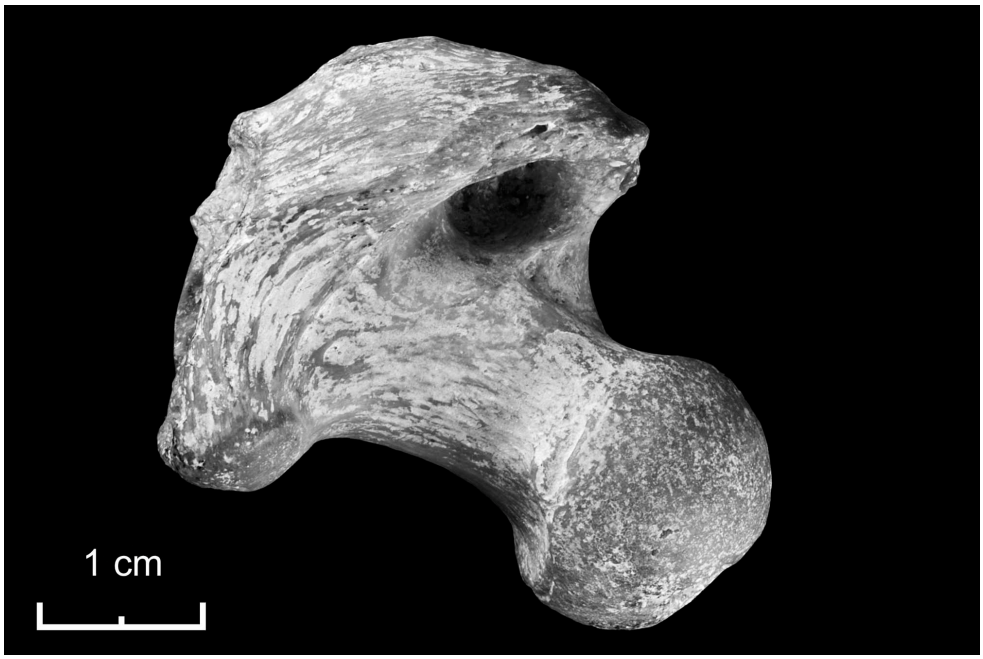

Figure A.53: Left femur fragment of *Pliopithecus vindobonensis* (O.E. 560), dorsal view

Figure A.54: Right and left femur of individuum II *Pliopithecus vindobonensis* (1970/1397/22, 1970/1397/23), ventral view

Figure A.55: Right and left femur of individuum II *Pliopithecus vindobonensis* (1970/1397/22, 1970/1397/23), dorsal view

Figure A.56: Left femur fragment of *Pliopithecus vindobonensis* (1970/1398/2), dorsal view

A.2.2 *Paidopithex rhenanus*

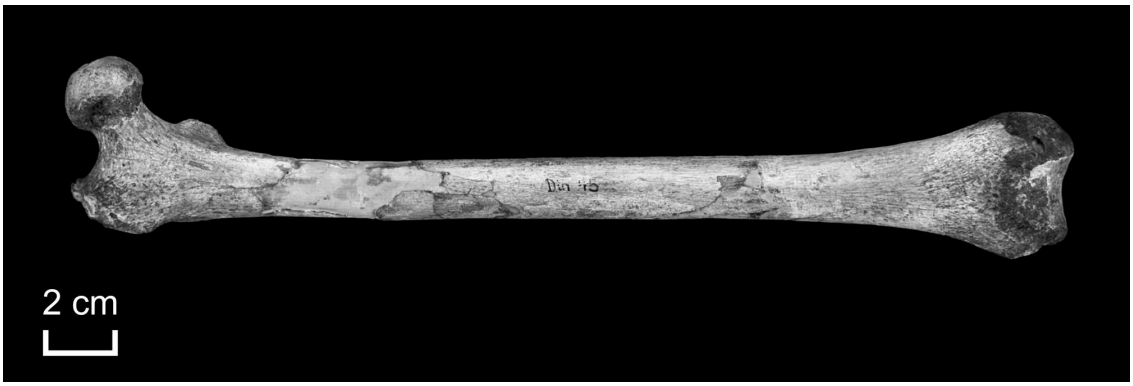

Figure A.57: Ventral view on the right femur of *Paidopithex rhenanus* (Din45)

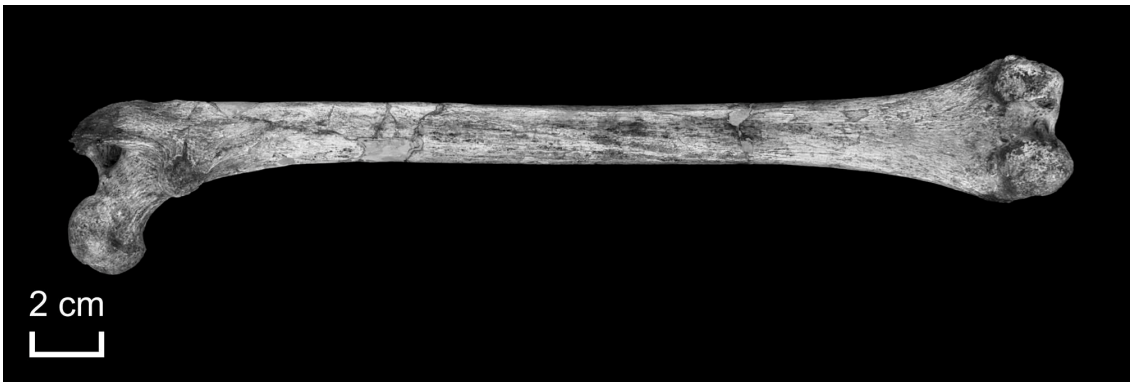

Figure A.58: Dorsal view on the right femur of *Paidopithex rhenanus* (Din45)

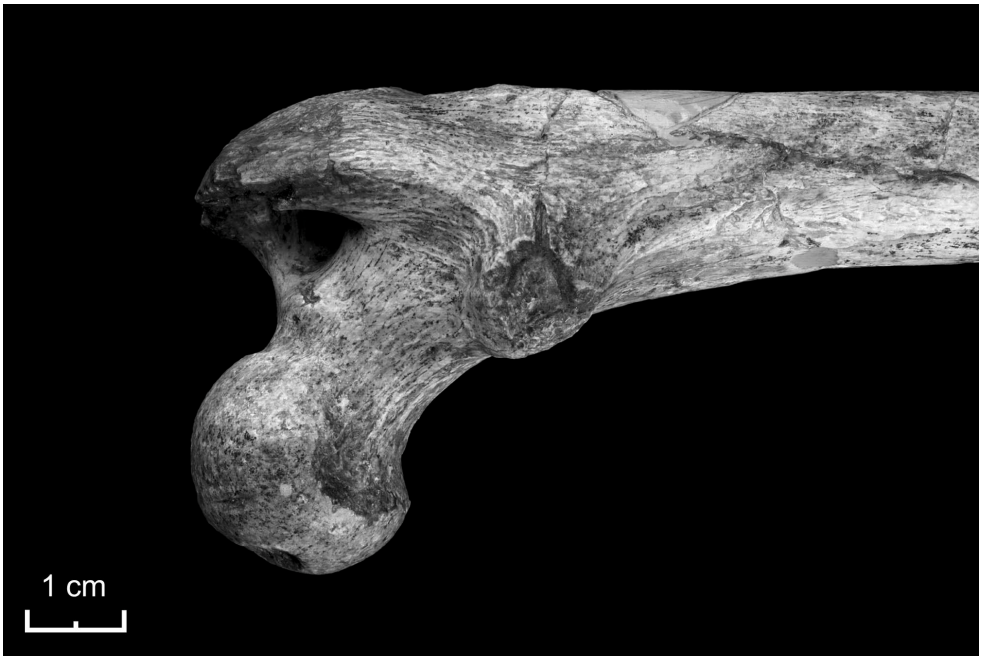

Figure A.59: Right femur of *Paidopithex rhenanus* (Din45), displaying the tuberculum on the posterior side of the neck

Appendix B

Data of bone surface morphometry

Table B.1: Results of morphometric measurements of *Alouatta seniculus* 69.19 l ♂

Measurement No.	1	2	3	4	5	**Average Value**
A [mm]	160.44	160.10	160.22	160.50	160.28	**160.31**
B [mm]	27.70	27.51	27.26	27.42	27.38	**27.45**
C [mm]	25.76	25.99	26.06	25.98	25.92	**25.94**
D [mm]	13.50	13.28	13.36	13.62	13.38	**13.43**
E [mm]	9.14	9.02	9.07	9.08	9.14	**9.09**
F [mm]	35.00	33.00	33.50	33.00	33.50	**33.60**
G_l [mm]	21.00	22.00	23.00	22.50	24.00	**22.50**
G_m [mm]	25.00	25.00	24.00	24.00	24.00	**24.40**
H [°]	137.38	134.87	135.00	139.83	138.33	**137.08**

Table B.2: Results of morphometric measurements of *Alouatta seniculus* 25 544 l ♀

Measurement No.	1	2	3	4	5	**Average Value**
A [mm]	151.48	151.66	151.62	151.60	151.60	**151.59**
B [mm]	24.05	24.06	24.02	24.00	23.99	**24.02**
C [mm]	23.09	23.14	23.12	22.90	22.90	**23.03**
D [mm]	12.96	12.76	12.96	12.90	12.99	**12.91**
E [mm]	9.86	9.64	9.82	9.66	9.62	**9.72**
F [mm]	31.00	31.00	30.00	30.50	31.00	**30.70**
G_l [mm]	23.00	22.00	23.00	23.00	23.00	**22.80**
G_m [mm]	26.00	26.00	25.00	26.00	27.00	**26.00**
H [°]	137.72	132.78	129.93	140.49	131.18	**134.42**

Table B.3: Results of morphometric measurements of *Alouatta seniculus* 25 545 l ♀

Measurement No.	1	2	3	4	5	**Average Value**
A [mm]	157.00	156.97	157.08	157.00	157.08	**157.30**
B [mm]	26.78	26.68	26.72	26.52	26.78	**26.70**
C [mm]	25.49	25.56	25.26	25.60	25.54	**25.49**
D [mm]	13.94	13.88	13.78	13.84	13.74	**13.84**
E [mm]	9.98	9.96	9.92	9.92	10.00	**9.96**
F [mm]	31.00	31.50	31.00	30.50	31.00	**31.00**
G_l [mm]	22.00	23.00	22.00	22.00	22.00	**22.20**
G_m [mm]	25.00	26.00	27.00	28.00	27.50	**26.70**
H [°]	136.86	123.96	135.01	133.85	139.20	**133.78**

Table B.4: Results of morphometric measurements of *Presbytis entellus* 4734 l

Measurement No.	1	2	3	4	5	**Average Value**
A [mm]	226.90	226.56	226.94	227.06	226.78	**226.85**
B [mm]	41.18	41.18	41.06	41.12	41.04	**41.12**
C [mm]	36.18	36.08	36.08	35.94	36.20	**36.10**
D [mm]	18.70	18.80	18.98	19.00	18.66	**18.83**
E [mm]	17.38	17.38	17.14	17.12	17.46	**17.30**
F [mm]	48.00	47.50	47.00	45.00	45.00	**46.50**
G_l [mm]	29.00	30.00	28.00	27.00	28.00	**28.40**
G_m [mm]	33.00	35.00	35.00	35.00	35.00	**34.60**
H [°]	140.39	136.04	140.29	139.65	142.40	**139.75**

Table B.5: Results of morphometric measurements of *Presbytis entellus* 4743 l

Measurement No.	1	2	3	4	5	**Average Value**
A [mm]	227.90	228.10	227.26	227.06	227.12	**227.49**
B [mm]	35.78	35.46	35.40	35.44	35.90	**35.60**
C [mm]	30.02	29.30	30.40	30.30	30.90	**30.18**
D [mm]	17.88	17.76	17.86	17.84	17.88	**17.84**
E [mm]	16.68	16.14	15.76	16.00	16.06	**16.13**
F [mm]	38.00	39.00	39.00	38.00	38.50	**38.50**
G_l [mm]	-	-	-	-	-	**-**
G_m [mm]	-	-	-	-	-	**-**
H [°]	-	-	-	-	-	**-**

Table B.6: Results of morphometric measurements of *Presbytis entellus* 4745 l

Measurement No.	1	2	3	4	5	**Average Value**
A [mm]	187.98	187.96	188.60	187.30	188.64	**188.10**
B [mm]	29.12	28.98	29.26	29.22	29.18	**29.15**
C [mm]	25.58	25.48	25.50	26.00	26.16	**25.74**
D [mm]	13.84	13.94	13.88	13.98	13.94	**13.92**
E [mm]	12.16	11.96	11.72	12.04	11.70	**11.92**
F [mm]	33.00	34.00	34.00	33.00	33.00	**33.40**
G_l [mm]	-	-	-	-	-	**-**
G_m [mm]	-	-	-	-	-	**-**
H [°]	139.24	132.37	134.55	136.95	137.18	**136.06**

Table B.7: Results of morphometric measurements of *Presbytis entellus* 4746 l

Measurement No.	1	2	3	4	5	**Average Value**
A [mm]	198.40	199.12	200.26	199.80	199.48	**199.41**
B [mm]	30.50	30.50	30.58	30.36	30.50	**30.49**
C [mm]	26.08	26.88	26.36	26.04	26.04	**26.28**
D [mm]	15.48	15.66	15.74	15.60	15.70	**15.64**
E [mm]	14.62	14.58	14.28	13.72	13.74	**14.19**
F [mm]	34.00	33.50	34.00	34.00	34.00	**33.90**
G_l [mm]	-	-	-	-	-	**-**
G_m [mm]	-	-	-	-	-	**-**
H [°]	128.33	127.46	132.91	129.16	135.44	**130.66**

Table B.8: Results of morphometric measurements of *Papio hamadryas* 1.553 l ♀

Measurement No.	1	2	3	4	5	**Average Value**
A [mm]	189.70	189.70	189.72	189.72	189.70	**189.71**
B [mm]	36.18	36.12	36.86	36.82	36.20	**36.44**
C [mm]	27.84	27.60	27.48	27.62	27.54	**27.62**
D [mm]	16.32	17.06	16.44	16.72	16.88	**16.68**
E [mm]	12.16	12.30	12.48	12.40	12.44	**12.36**
F [mm]	38.00	37.00	37.50	38.00	38.00	**37.70**
G_l [mm]	28.00	25.00	27.00	27.00	26.00	**26.60**
G_m [mm]	31.00	32.00	32.00	32.50	32.00	**31.90**
H [°]	136.74	131.67	125.38	137.87	132.28	**132.79**

Table B.9: Results of morphometric measurements of *Papio hamadryas* HA VIII 3 l ♂

Measurement No.	1	2	3	4	5	**Average Value**
A [mm]	220.58	220.64	220.64	220.64	220.66	**220.63**
B [mm]	43.40	43.44	43.60	43.22	43.28	**43.39**
C [mm]	35.08	34.68	34.66	34.22	34.32	**34.59**
D [mm]	19.38	19.46	19.44	19.30	19.70	**19.46**
E [mm]	15.34	14.92	15.36	15.36	15.00	**15.20**
F [mm]	49.00	48.00	44.00	48.00	48.00	**47.40**
G_l [mm]	34.00	33.00	32.00	32.00	33.50	**32.90**
G_m [mm]	43.00	41.00	40.00	41.00	40.50	**41.10**
H [°]	139.99	126.37	135.13	136.38	137.87	**135.15**

Table B.10: Results of morphometric measurements of *Papio hamadryas* HA VIII 83 l ♂

Measurement No.	1	2	3	4	5	**Average Value**
A [mm]	249.30	249.12	249.28	249.24	249.52	**249.29**
B [mm]	46.90	47.10	47.00	47.20	47.06	**47.05**
C [mm]	36.70	36.88	36.96	36.98	36.94	**36.89**
D [mm]	20.38	21.20	21.44	20.86	21.28	**21.03**
E [mm]	16.24	15.82	16.46	16.12	16.60	**16.25**
F [mm]	49.00	49.00	49.00	48.00	48.00	**48.60**
G_l [mm]	33.00	32.00	33.00	32.00	32.00	**32.40**
G_m [mm]	35.00	39.50	39.00	39.00	40.00	**38.50**
H [°]	129.91	127.69	140.06	139.83	137.27	**134.95**

Table B.11: Results of morphometric measurements of *Papio hamadryas* 3212 l ♂

Measurement No.	1	2	3	4	5	**Average Value**
A [mm]	241.74	241.74	241.72	241.74	241.78	**241.74**
B [mm]	47.20	47.04	46.18	47.16	47.10	**46.94**
C [mm]	37.06	37.06	37.08	37.10	37.00	**37.06**
D [mm]	21.96	22.16	21.86	22.00	22.00	**22.00**
E [mm]	16.00	15.98	16.28	16.12	16.68	**16.21**
F [mm]	50.00	49.00	48.00	50.00	50.00	**49.40**
G_l [mm]	31.00	32.00	32.00	33.00	33.00	**32.20**
G_m [mm]	42.00	41.00	40.00	41.00	40.50	**40.90**
H [°]	131.50	136.43	128.49	129.91	133.65	**132.00**

Table B.12: Results of morphometric measurements of *Hylobates lar moloch* 47 979 r ♂

Measurement No.	1	2	3	4	5	**Average Value**
A [mm]	203.54	203.74	203.60	203.84	203.74	**203.69**
B [mm]	29.00	29.36	29.14	29.50	29.04	**29.21**
C [mm]	26.58	26.40	26.70	26.52	26.62	**26.56**
D [mm]	15.38	15.40	15.82	15.10	15.18	**15.38**
E [mm]	11.38	10.62	10.42	10.75	10.66	**10.77**
F [mm]	32.00	33.00	32.00	32.00	32.50	**32.30**
G_l [mm]	25.00	25.00	27.00	24.50	26.50	**25.60**
G_m [mm]	30.00	29.00	28.00	28.00	28.00	**28.60**
H [°]	136.88	144.66	140.84	143.97	138.58	**140.99**

Table B.13: Results of morphometric measurements of *Hylobates syndactylus* 6983 l ♂

Measurement No.	1	2	3	4	5	**Average Value**
A [mm]	205.58	205.56	205.30	205.50	205.58	**205.50**
B [mm]	31.38	31.48	31.38	31.56	31.20	**31.40**
C [mm]	27.58	27.78	28.04	27.92	27.78	**27.82**
D [mm]	17.78	18.06	18.08	17.99	17.88	**17.96**
E [mm]	9.99	10.54	9.84	10.14	10.30	**10.16**
F [mm]	34.00	35.00	35.00	36.00	35.00	**35.00**
G_l [mm]	27.00	27.00	28.00	27.00	27.00	**27.20**
G_m [mm]	33.00	32.00	32.00	31.50	32.00	**32.10**
H [°]	144.99	146.26	144.43	140.64	147.09	**144.58**

Table B.14: Results of morphometric measurements of *Hylobates syndactylus* 52.36 l ♀

Measurement No.	1	2	3	4	5	**Average Value**
A [mm]	212.64	212.74	212.60	212.24	212.66	**212.58**
B [mm]	35.18	35.69	35.30	35.50	35.54	**35.44**
C [mm]	32.16	32.10	32.02	32.16	32.08	**32.10**
D [mm]	18.72	18.70	18.94	18.52	18.74	**18.72**
E [mm]	11.67	11.80	11.54	11.60	11.88	**11.70**
F [mm]	38.00	38.00	38.00	38.00	38.00	**38.00**
G_l [mm]	28.00	27.00	30.00	29.00	29.00	**28.60**
G_m [mm]	34.00	32.00	34.00	33.00	34.00	**33.40**
H [°]	141.32	148.09	144.30	140.90	142.41	**143.40**

Table B.15: Results of the morphometric measurements of *Homo sapiens* 10 l ♀

Measurement No.	1	2	3	4	5	**Average Value**
A [mm]	434.00	435.00	437.00	436.00	434.00	**435.20**
B [mm]	83.68	82.90	84.08	83.44	81.98	**83.22**
C [mm]	72.94	72.98	72.96	72.66	73.14	**72.94**
D [mm]	40.00	39.82	40.80	39.38	41.14	**40.23**
E [mm]	32.94	32.76	32.82	32.96	33.00	**32.90**
F [mm]	82.00	83.00	83.00	82.00	82.00	**82.40**
G_l [mm]	56.00	59.00	58.00	58.00	55.00	**57.20**
G_m [mm]	71.00	70.00	72.00	70.00	69.00	**70.40**
H [°]	135.79	143.87	134.49	139.65	139.51	**138.66**

Table B.16: Results of the morphometric measurements of *Homo sapiens* 11 l ♂

Measurement No.	1	2	3	4	5	**Average Value**
A [mm]	507.00	504.00	504.00	508.00	503.00	**505.20**
B [mm]	101.28	100.69	100.55	101.34	100.94	**100.96**
C [mm]	85.40	84.85	84.80	86.64	84.92	**85.32**
D [mm]	48.54	50.52	50.32	50.94	48.94	**49.85**
E [mm]	40.37	40.20	40.54	40.22	40.50	**40.37**
F [mm]	95.00	94.00	96.00	94.00	93.00	**94.40**
G_l [mm]	66.00	66.00	67.00	72.00	67.00	**67.60**
G_m [mm]	83.00	79.00	82.00	82.00	80.00	**81.20**
H [°]	133.67	134.02	136.34	135.26	136.44	**135.15**

Table B.17: Results of the morphometric measurements of *Homo sapiens* 21 l ♂

Measurement No.	1	2	3	4	5	**Average Value**
A [mm]	513.00	513.00	512.00	514.00	517.00	**513.80**
B [mm]	108.78	110.30	109.16	110.44	109.58	**109.65**
C [mm]	94.60	94.66	93.81	93.84	93.88	**94.16**
D [mm]	50.54	50.46	50.52	50.32	51.06	**50.58**
E [mm]	38.90	39.32	38.84	38.54	38.90	**38.90**
F [mm]	97.00	99.00	97.00	98.00	98.00	**97.80**
G_l [mm]	72.00	69.00	66.00	68.00	68.00	**68.60**
G_m [mm]	81.00	82.00	82.00	84.00	87.00	**83.20**
H [°]	131.82	127.45	134.58	133.08	129.78	**131.34**

Table B.18: Results of the morphometric measurements of *Homo sapiens* 22 l ♀

Measurement No.	1	2	3	4	5	**Average Value**
A [mm]	425.00	423.00	423.00	424.00	424.00	**423.80**
B [mm]	75.68	74.90	76.30	78.40	77.10	**76.46**
C [mm]	69.10	68.96	68.86	68.78	68.94	**68.93**
D [mm]	36.98	36.69	36.42	37.26	37.04	**36.88**
E [mm]	25.70	27.34	26.70	25.90	26.38	**26.40**
F [mm]	78.00	79.00	80.00	79.00	80.00	**79.20**
G_l [mm]	60.00	57.00	57.00	56.00	57.00	**57.40**
G_m [mm]	73.00	70.00	74.00	76.00	75.00	**73.60**
H [°]	141.45	142.81	138.14	142.07	139.39	**140.77**

Table B.19: Results of the morphometric measurements of *Pliopithecus vindobonensis* individuum I O.E. 304 r

Measurement No.	1	2	3	4	5	**Average Value**
A [mm]	215.42	215.76	216.18	215.68	215.56	**215.72**
B [mm]	36.28	36.84	37.50	36.68	36.92	**36.84**
C [mm]	34.66	34.22	33.94	34.56	34.68	**34.41**
D [mm]	16.88	17.08	16.96	17.18	16.80	**16.98**
E [mm]	12.90	12.76	12.56	12.72	12.70	**12.73**
F [mm]	40.00	40.20	39.90	40.30	40.40	**40.16**
G_l [mm]	28.00	29.00	28.80	28.80	29.00	**28.72**
G_m [mm]	32.00	33.00	32.00	32.20	32.00	**32.24**
H [°]	131.72	138.42	132.13	129.89	132.39	**132.91**

Table B.20: Results of the morphometric measurements of *Pliopithecus vindobonensis* O.E. 559 l

Measurement No.	1	2	3	4	5	**Average Value**
A [mm]	-	-	-	-	-	**-**
B [mm]	37.24	36.68	36.78	37.54	37.54	**37.16**
C [mm]	-	-	-	-	-	**-**
D [mm]	16.28	16.84	16.28	16.20	16.70	**16.46**
E [mm]	13.00	12.82	12.76	12.76	12.90	**12.85**
F [mm]	-	-	-	-	-	**-**
G_l [mm]	-	-	-	-	-	**-**
G_m [mm]	-	-	-	-	-	**-**
H [°]	139.19	142.55	136.30	132.71	140.71	**138.29**

Table B.21: Results of the morphometric measurements of *Pliopithecus vindobonensis* O.E. 560 l

Measurement No.	1	2	3	4	5	**Average Value**
A [mm]	-	-	-	-	-	**-**
B [mm]	36.16	36.88	36.94	36.72	36.30	**36.60**
C [mm]	-	-	-	-	-	**-**
D [mm]	16.00	15.62	15.60	16.08	16.06	**15.87**
E [mm]	12.36	12.16	12.22	12.20	12.18	**12.22**
F [mm]	-	-	-	-	-	**-**
G_l [mm]	-	-	-	-	-	**-**
G_m [mm]	-	-	-	-	-	**-**
H [°]	136.11	126.96	124.10	140.59	138.51	**133.25**

Table B.22: Results of the morphometric measurements of *Pliopithecus vindobonensis* individuum II 1970/1397/22 r

Measurement No.	1	2	3	4	5	**Average Value**
A [mm]	206.32	206.26	206.30	206.32	206.12	**206.26**
B [mm]	37.96	38.34	37.86	38.38	38.26	**38.16**
C [mm]	30.68	30.70	30.80	30.70	30.78	**30.73**
D [mm]	17.18	16.98	16.98	17.34	17.40	**17.18**
E [mm]	12.76	12.70	12.56	12.80	12.82	**12.73**
F [mm]	36.30	36.00	36.50	36.50	36.20	**36.30**
G_l [mm]	32.50	33.00	32.00	31.50	32.00	**32.20**
G_m [mm]	34.00	33.00	34.00	32.50	33.50	**33.40**
H [°]	130.59	128.37	131.72	127.27	130.89	**129.77**

Table B.23: Results of the morphometric measurements of *Pliopithecus vindobonensis* individuum II 1970/1397/23 l

Measurement No.	1	2	3	4	5	**Average Value**
A [mm]	205.78	205.82	205.96	205.90	206.16	**205.924**
B [mm]	37.16	37.22	37.44	37.26	37.76	**37.37**
C [mm]	30.86	30.98	30.98	31.16	30.98	**30.99**
D [mm]	16.72	16.64	16.62	16.44	16.28	**16.54**
E [mm]	12.98	12.48	12.56	12.64	12.52	**12.64**
F [mm]	35.60	35.80	36.00	35.50	35.30	**35.64**
G_l [mm]	33.00	32.00	33.00	31.00	32.50	**33.20**
G_m [mm]	33.50	33.00	33.00	33.00	33.50	**32.20**
H [°]	133.25	134.09	138.79	135.14	134.96	**135.25**

Table B.24: Results of the morphometric measurements of *Pliopithecus vindobonensis* 1970/1398/2 l

Measurement No.	1	2	3	4	5	**Average Value**
A [mm]	-	-	-	-	-	**-**
B [mm]	36.98	36.32	36.40	37.00	36.74	**36.69**
C [mm]	-	-	-	-	-	**-**
D [mm]	15.88	16.02	15.98	16.08	15.74	**15.94**
E [mm]	13.00	12.98	13.22	13.06	12.86	**13.02**
F [mm]	38.00	38.50	37.80	38.00	38.00	**38.06**
G_l [mm]	-	-	-	-	-	**-**
G_m [mm]	-	-	-	-	-	**-**
H [°]	132.52	131.14	129.43	138.53	135.02	**133.33**

Table B.25: Results of the morphometric measurements of the dextral femur of *Paidopithex rhenanus* DIN 45 r

Measurement No.	1	2	3	4	5	**Average Value**
A [mm]	283.47	281.72	283.20	283.00	282.40	**282.76**
B [mm]	50.20	49.90	49.80	49.83	49.52	**49.85**
C [mm]	41.33	41.28	40.49	41.06	41.18	**41.07**
D [mm]	22.00	22.30	22.10	22.20	22.04	**22.13**
E [mm]	17.20	16.80	16.90	16.88	16.97	**16.95**
F [mm]	58.00	59.00	58.50	58.00	58.00	**58.30**
G_l [mm]	32.00	33.00	34.00	32.50	32.50	**32.80**
G_m [mm]	35.00	35.00	35.00	37.00	36.00	**35.60**
H [°]	136.83	140.81	137.99	138.62	140.68	**138.99**

Table B.26: The average values over five morphometric measurements of each parameter of the extant species

	A [mm]	B [mm]	C [mm]	D [mm]	E [mm]	F [mm]	G_l [mm]	G_m [mm]	H [°]
Alouatta s. (69.19 l) ♂	160.31	27.45	25.94	13.43	9.09	33.60	22.50	24.40	137.08
Alouatta s. (25 544 l) ♀	151.59	24.04	23.03	12.91	9.72	30.70	22.80	26.00	134.42
Alouatta s. (25 545 l) ♀	157.30	26.70	25.49	13.84	9.96	31.00	22.20	26.70	133.78
Presbytis e. (4734 l)	226.85	41.12	36.10	18.83	17.30	46.50	28.40	34.60	139.75
Presbytis e. (4743 l)	227.49	35.60	30.18	17.84	16.13	38.50	-	-	-
Presbytis e. (4745 l)	188.10	29.15	25.74	13.92	11.92	33.40	-	-	136.06
Presbytis e. (4746 l)	199.41	30.49	26.28	15.64	14.19	33.90	-	-	130.66
Papio h. (1.553 l) ♀	189.71	36.44	27.62	16.68	12.36	37.70	26.60	31.90	132.79
Papio h. (HA VIII 3 l) ♂	220.63	43.39	34.59	19.46	15.20	47.40	32.90	41.10	135.15
Papio h. (HA VIII 83 l) ♂	249.29	47.05	36.89	21.03	16.25	48.60	32.40	38.50	134.95
Papio h. (3212 l) ♂	241.74	46.94	37.06	22.00	16.21	49.40	32.20	40.90	132.00
Hylobates l. m. (47 979 l) ♂	203.69	29.21	26.56	15.38	10.77	32.30	25.60	28.60	140.99
Hylobates s. (6983 l) ♂	205.50	31.40	27.82	17.96	10.16	35.00	27.20	32.10	144.58
Hylobates s. (52.36 l) ♀	212.58	35.44	32.10	18.72	11.70	38.00	28.60	33.40	143.40
Homo s. (10 l) ♀	435.20	83.22	72.94	40.23	32.90	82.40	57.20	70.40	138.66
Homo s. (11 l) ♂	505.20	100.96	85.32	49.85	40.37	94.40	67.60	81.20	135.15
Homo s. (21 l) ♂	513.80	109.65	94.16	50.58	38.90	97.80	68.60	83.20	131.34
Homo s. (22 l) ♀	423.80	76.46	68.93	36.88	26.40	79.20	57.40	73.60	140.77

Table B.27: The average values over five morphometric measurements of each parameter of the fossil species

	A [mm]	B [mm]	C [mm]	D [mm]	E [mm]	F [mm]	G_l [mm]	G_m [mm]	H [°]
Pliopithecus v. (O.E. 304 r)	215.72	36.84	34.41	16.98	12.73	40.16	28.72	32.24	132.91
Pliopithecus v. (O.E. 559 l)	-	36.60	-	15.87	12.22	-	-	-	138.29
Pliopithecus v. (O.E. 560 l)	-	37.16	-	16.46	12.85	-	-	-	133.25
Pliopithecus v. (1970/1397/22 r)	206.26	38.16	30.73	17.18	12.73	36.30	32.20	33.40	129.77
Pliopithecus v. (1970/1397/23 l)	205.92	37.37	30.99	16.54	12.64	35.64	32.30	33.20	135.25
Pliopithecus v. (1970/1398/2 l)	-	36.69	-	15.94	13.02	38.06	-	-	133.33
Paidopithex r. (Din 45 r)	282.76	49.85	41.07	22.13	16.95	58.30	32.80	35.60	138.99

Appendix C

Data of CT image histomorphometry

Table C.1: The results of the histomorphometric analysis of the ROI of the extant species

	TV [mm^3]	BV [mm^3]	BV/TV [mm^3]	Conn.Dens [$1/mm^3$]	SMI [1]	|H1| [mm]	|H2| [mm]	|H3| [mm]
Alouatta s. (69.19 l) ♂	916.1970	111.7919	0.1220	0.5075	0.5179	1.3855	2.1604	1.5728
Alouatta s. (25 544 l) ♀	512.6947	148.3304	0.2843	2.9246	-0.1721	0.6010	0.9012	0.6403
Alouatta s. (25 545 l) ♀	655.3165	104.4962	0.1595	0.9167	0.0204	1.0895	1.5898	1.1520
Presbytis e. (4734 l)	2387.2852	916.7345	0.3840	1.2776	-1.2336	0.6853	1.1092	0.7892
Presbytis e. (4745 l)	789.1430	161.9140	0.2052	2.4191	0.3197	0.7342	1.4657	0.9191
Presbytis e. (4746 l)	920.2951	273.2180	0.2969	3.2881	-0.5274	0.5679	1.0253	0.6639
Papio h. (1.553 l) ♀	1127.2950	228.3930	0.2026	1.5378	0.7018	0.8521	1.1067	0.9004
Papio h. (HA VIII 3 l) ♂	1906.5837	464.7419	0.2438	0.8977	0.0773	0.9020	1.3201	1.0599
Papio h. (HA VIII 83 l) ♂	2390.4304	648.0010	0.2711	1.1855	-0.2664	0.7903	1.2449	0.8885
Papio h. (3212 l) ♂	2004.0785	451.6277	0.2254	0.9652	0.1007	0.8491	1.3872	1.0894
Hylobates l. m. (47 979 l) ♂	883.4962	112.4098	0.1272	0.4216	0.0078	1.2115	2.2773	1.4595
Hylobates s. (6983 l) ♂	686.0164	234.5587	0.3419	2.2995	-0.5846	0.6491	1.0335	0.7282
Hylobates s. (52.36 l) ♀	1229.5940	355.3277	0.2890	1.5056	-0.2553	0.7291	1.0956	0.7819
Homo s. (10 l) ♀	16614.0117	4995.4287	0.3007	0.7582	0.8914	1.0259	1.6206	1.2043
Homo s. (11 l) ♂	28547.2129	12322.7158	0.4317	0.4231	-0.4022	1.1385	1.8811	1.3195
Homo s. (21 l) ♂	22823.8848	13543.1211	0.5934	0.2277	-3.7335	1.1499	1.9626	1.3036
Homo s. (22 l) ♀	9322.3525	3027.5510	0.3248	0.5391	0.2707	1.2315	2.1781	1.4298

	DA [1]	Tb.Th [mm]	Tb.Th SD [mm]	Tb.Sp [mm]	Tb.Sp SD [mm]	Tb.N [1/mm]	BS [mm^2]
Alouatta s. (69.19 l) ♂	1.5596	0.2537	0.1209	1.7754	0.8534	0.5416	1104.2316
Alouatta s. (25 544 l) ♀	1.4995	0.2280	0.0820	0.8702	0.4752	1.1083	1495.1882
Alouatta s. (25 545 l) ♀	1.4592	0.2993	0.0864	1.8419	1.1879	0.5640	1054.0977
Presbytis e. (4734 l)	1.6187	0.3498	0.1297	1.0760	1.0184	0.9590	5801.8433
Presbytis e. (4745 l)	1.9963	0.2420	0.1000	1.6115	1.3284	0.6612	1661.5156
Presbytis e. (4746 l)	1.8054	0.2390	0.0798	0.9223	0.7494	1.1023	2602.8513
Papio h. (1.553 l) ♀	1.2988	0.2441	0.1178	1.0528	0.6378	0.9632	2370.9028
Papio h. (HA VIII 3 l) ♂	1.4635	0.3289	0.1595	1.1318	0.6776	0.8964	3536.1523
Papio h. (HA VIII 83 l) ♂	1.5752	0.2999	0.1194	1.2492	1.1720	0.8368	5037.8745
Papio h. (3212 l) ♂	1.6337	0.2966	0.1369	1.5884	1.5417	0.6819	3771.8340
Hylobates l. m. (47 979 l) ♂	1.8798	0.2183	0.0861	2.3115	1.3998	0.4526	1156.5883
Hylobates s. (6983 l) ♂	1.5922	0.3020	0.1010	1.0281	0.6909	1.0235	1776.5068
Hylobates s. (52.36 l) ♀	1.5027	0.2911	0.1123	1.0015	0.5143	0.9752	2893.4668
Homo s. (10 l) ♀	1.5797	0.4736	0.3081	1.1304	0.6459	0.8801	26690.0403
Homo s. (11 l) ♂	1.6523	0.7277	0.4457	1.2911	0.8652	0.7677	41170.3635
Homo s. (21 l) ♂	1.7067	0.8219	0.3981	0.9496	0.4949	0.9114	32662.2971
Homo s. (22 l) ♀	1.7686	0.5875	0.3340	3.3986	4.3645	0.3698	12316.2577

Table C.2: The results of the histomorphometric analysis of the ROI of the fossil species

	TV [mm^3]	BV [mm^3]	BV/TV [mm^3]	Conn.Dens [$1/mm^3$]	SMI [1]	|H1| [mm]	|H2| [mm]	|H3| [mm]
Pliopithecus v. (O.E. 304 r)	1463.4131	424.6105	0.2902	2.8543	-0.7187	0.6563	0.8381	0.6859
Pliopithecus v. (O.E. 559 l)	1532.8043	494.3640	0.3225	2.4592	-1.1061	0.6565	0.8899	0.6749
Pliopithecus v. (1970/1397/22 r)	1110.4897	327.7403	0.2951	4.5052	-0.2760	0.5864	0.8200	0.6877
Pliopithecus v. (1970/1397/23 l)	1004.5920	319.8708	0.3184	3.9743	-0.5092	0.6101	0.8845	0.6573
Pliopithecus v. (1970/1398/2 l)	1669.8541	523.2320	0.3133	2.7359	-0.7415	0.6445	0.8698	0.6544
Paidopithex r. (Din 45 r)	3948.7432	1096.8416	0.2770	0.6795	-1.2845	0.8908	1.4323	1.0319

	DA [1]	Tb.Th [mm]	Tb.Th SD [mm]	Tb.Sp [mm]	Tb.Sp SD [mm]	Tb.N [1/mm]	BS [mm^2]
Pliopithecus v. (O.E. 304 r)	1.2769	0.2239	0.0713	1.0196	0.7582	1.0469	4041.1841
Pliopithecus v. (O.E. 559 l)	1.3554	0.2511	0.0879	1.0920	0.8338	0.9659	4192.2700
Pliopithecus v. (1970/1397/22 r)	1.3983	0.2138	0.0699	0.9887	0.9295	1.1298	3320.3513
Pliopithecus v. (1970/1397/23 l)	1.4498	0.2417	0.0798	1.0019	0.7975	1.0212	2855.4985
Pliopithecus v. (1970/1398/2 l)	1.3496	0.2347	0.0696	0.9014	0.5044	1.1000	4682.6514
Paidopithex r. (Din 45 r)	1.6079	0.3250	0.1287	2.3763	2.2335	0.4742	7355.2764

Bibliography

Aaron, J. & Skerry, T.M. (1994) Intermembranous trabecular generation in normal bone. *Bone and Mineral*, 25, pp. 211-230.

Adler, C.-P. (1998) Knochenkrankheiten. *Springer Verlag; 2. Auflage*, pages 1-591.

Aiello L.C. (1981) Locomotion in the miocene hominoidea. *in: Aspects of Human Evolution; Stringer, C.B. (ed.); Taylor & Francis LTD*, pages 63-97.

Aiello, L. & Dean, C. (1990) An introduction to human evolutionary anatomy. *Academic Press*, pages 1-596.

Andrews, P.; Harrison, T.; Delson, E., Bernor, R.L.; Martin, L. (1996) Distribution and biochronology of european and southwest asian Miocene catarrhines. *in: The Evolution of Western Eurasian Neogene Mammal Faunas; Bernor, R.L.; Fahlbusch, V.; Mittmann, H.-W. (eds.); Columbia University Press*, pages 168-207.

Ankel, F. (1965) Der Canalis sacralis als Indikator für die Länge der Caudalregion der Primaten. *Folia Primatologica*, 3, pp. 263-276.

Ashton, E.H. & Oxnard, C.E. (1964) Locomotor patterns in primates. *Proceedings of the Zoological Society London*, 142[1], pp. 1-28.

Audebert, J.B. (1798) Histoire naturelle des signes et des makis. *Desray.*

Baldwin, L.A. & Teleki, G. (1976) Patterns of gibbon behavior on Hall's Island, Bermuda. *Gibbon and Siamang*, 4, pp. 21-105.

Barrett, L. (2000) Baboons. *BBC Worldwide Ltd.*, pages 1-96.

Beaupré, G.S.; Orr, T.E.; Carter, D.R. (1990a) An approach for time-dependent bone modeling and remodeling - theoretical development. *Journal of Orthopaedic Research*, 8, pp. 651-661.

Beaupré, G.S.; Orr, T.E.; Carter, D.R. (1990b) An approach for time-dependent bone modeling and remodeling-application: A preliminary remodeling simulation. *Journal of Orthopaedic Research*, 8, pp. 662-670.

Becker, R.O.; Bassett, C.A.; Bachman, C.H. (1964) Bioelectrical factors controlling bone structure. *in: Bone Biodynamics; Frost, H.M. (ed.); Little, Brown and Company*, pages 209-232.

Begun, D.R. (1992) Phyletic diversity and locomotion in primitive european hominids. *American Journal of Physical Anthropology*, 87, pp. 311-340.

Bergeson, D.J. (1998) Patterns of suspensory feeding in *Alouatta palliata*, *Ateles geoffroyi*, and *Cebus capucinus*. *in: Primate Locomotion: Recent Advances Strasser, E.; Fleagle, J.; Rosenberger, A.; McHenry, H. (eds.); Plenum Press*, pages 45-60.

Bergmann, G.; Graichen, F.; Rohlmann, A. (1993) Hip joint loading during walking and running, measured in two patients. *Journal of Biomechanics*, 26[8], pp. 969-990.

Biewener, A.A. (1989) Scaling body support in mammals: Limb posture and muscle mechanics. *Science*, 245, pp. 45-48.

Blyth, E. (1875) Catalogue of mammals and birds of Burma. *Journal of the Asiatic Society of Bengal*, 44, (Part 2, extra number), pp. 1-167.

Bonse, U.; Busch, F.; Günnewig, O.; Beckmann, F.; Pahl, R.; Delling, G.; Hahn, M.; Graeff, W. (1994) 3D computed X-ray tomography of human cancellous bone at 8 μm spatial and 10 $^{-4}$ energy resolution. *Bone and Mineral*, 25, pp. 25-38.

Borah, B.; Gross, G.J.; Dufresne, T.E.; Smith, T.S.; Cockman, M.D.; Chmielewski, P.A.; Lundy, M.W.; Hartke J.J.; Sod, E.W. (2001) Three-dimensional microimaging (MrμI and μCT), finite element modeling, and rapid, prototyping provide unique insight into bone architecture in osteoporosis. *The Anatomical Record (New Anat.)*, 265, pp. 101-110.

Brand, R.A.; Pedersen, D.R.; Friedrich, J.A. (1986) The sensitivity of muscle force predictions to changes in physiologic cross-sectional area. *Journal of Biomechanics*, 19[6], pp. 589-596.

Carpenter, C.R. (1934) A field study of the behavior and social relations of howling monkeys (*Alouatta palliata*). *Comparative Psychology Monographs; The John Hopkins Press*, X, pp. 1-168.

Carpenter, C.R. (1940) A field study in Siam of the behavior and social relations of the gibbon (*Hylobates lar*). *reprinted in: Naturalistic behavior of non-human primates; Carpenter, C.R.; University Park: Penn. State U. Press 1964*, pages 145-271.

Carter, D.R.; Fyhrie; D.P.; Whalen, R.T. (1987) Trabecular bone density and loading history: regulation of connective tissue biology by mechanical energy. *Journal of Biomechanics*, 20[8], pp. 785-794.

Chambers, T.J.; Evans, M.; Gardner, T.N.; Turner-Smith, A.; Chow, J.W.M. (1993) Induction of bone formation in rat tail vertebrae by mechanical loading. *Bone and Mineral*, 20, pp. 167-178.

Cheal, E.J.; Snyder, B.D.; Nunamaker, D.M.; Hayes, W.C. (1987) Trabecular bone remodeling around smooth and porous implants in an equine patellar model. *Journal of Biomechanics*, 20[11/12], pp. 1121-1134.

Ciochon, R.L. & Corruccini, R.S. (1977) The phenetic position of *Pliopithecus* and its phylogenetic relationship to the hominoidea. *Systematic Zoology*, 26, pp. 290-299.

Compston, J.E. (1994) Connectivity of cancellous bone: Assessment and mechanical implications. *Bone*, 15[5], pp. 463-466.

Conroy, G.C. (1990) Primate evolution. *W.W. Norton & Company*, pages 1-492.

Conroy, G.C. (1997) Reconstructing human origins. *W.W. Norton & Company*, pages 1-557.

Copf, F. (2001) Auf dem Weg zu einer neuen bionischen Endoprothese des Hüftgelenks. *in: BIONA-report 15; Wisser, A.; Nachtigall,W. (eds.); Akademie der Wissenschaften und der Literatur*, pages 91-119.

Copf, F. & Czarnetzki, A. (1989) Two-membrane system in the caput femoris and the distal femoral condyles. *Acta Anatomica*, 136, pp. 255-256.

Copf, F. & Holz, U. (eds.) (1994) Knochen als dynamisches Prinzip. *Georg Thieme Verlag*, pages 1-167.

Cowin, S.C. (2001) Bone poroelasticity. *in: Bone Mechanics Handbook 2. Ed.; Cowin, S.C. (ed.); CRC Press*, pages 23-1 - 23-31.

Cowin, S.C.; Moss-Salentjin, L.; Moss, M.L. (1991) Candidates for the mechanosensory system in bone. *Journal of Biomechanical Engineering*, 113, pp. 191-197.

Cowin, S.C.; Sadegh, A.M.; Luo, G.M. (1992) An evolutionary Wolff's law for trabecular architecture. *Journal of Biomechanical Engineering*, 114, pp. 129-136.

Crowninshield, R.D.; Johnston, R.C.; Andrews, J.G.; Brand, R.A. (1978) A biomechanical investigation of the human hip. *Journal of Biomechanics*, 11, pp. 75-85.

Dalstra, M.; Beckmann, F.; Melsen, F.; Hauge, E.M.; Hoffmann, S.V.; Lunt, S.; Uggerhoj, E. (1999) High-resolution CT scanning of bone using synchrotron radiation. *HASYLAB Annual Report online.*

Davy, D.T.; Kotzar, G.M.; Brown, R.H.; Heiple, K.G.; Goldberg, V.M.; Heiple jr., K.G.; Berilla, J.; Burstein, A.H. (1988) Telemetric, force measurements across the hip after total arthroplasty. *The Journal of Bone and Joint Surgery*, 70-A[1], pp. 45-50.

Daxner-Höck, G. (1998) Säugetiere (Mammalia) aus dem Karpat des Korneuburger Beckens 3. Rodentia und Carnicora. *Beiträge zur Paläontologie*, 23, pp. 367-407.

Day, M.H. (1979) The locomotor interpretation if fossil primate postcranial bones. *in: Environment, Behavior, And Morphology: Dynamic Interactions in Primates; Morbeck, M.E.; Preuschoft, H.; Gomberg, N. (eds.); Gustav Fischer Verlag*, pages 245-258.

Dempster, D.W. (1992) Bone remodeling. *in: Disorders of Bone and Mineral Metabolism; Coe, F.L.; Favus, M.J. (eds.); Raven Press*, pages 355-380.

Die Affen - Neuweltaffen in Südamerika. (1990) *REVCOM and Bayrischer Rundfunk.*

Die Affen - Paviane und Mantelaffen in Afrika (1990) *REVCOM and Bayrischer Rundfunk.*

Draenert, K. (1986) Der Knochen als hydraulisches System. *Konzepte SFB*, 230[14], pp. 63-71.

von den Driesch, A. (1982) Das Vermessen von Tierknochen aus vor- und fr"uhgeschichtlichen Siedlungen. *Institut f"ur Pal"aoanatomie, Domestikationsforschung und Geschichte der Tiermedizin der Universit"at M"unchen*, pages 1-114.

Dubois, E. (1895) Le Pithecanthropus erectus du Pliocène de Java. *Bulletin de la Société Belge de Géologie*, IX, pp. 151-160.

Duerst, J.U. (1926) Vergleichende Untersuchungsmethoden am Skelett bei Säugern. *Handbuch der biologischen Arbeitsmethoden*, (Teil 1), pages 125-530.

Duda, G.N. (1996) Influence of muscle forces on the internal loads in the femur during gait. *Dissertation Hamburg-Harburg, Shaker Verlag*, pages 1-189.

Duda, G.N.; Heller, M.; Albiger, J.; Schulz, O.; Schneider, E.; Claes, L. (1998) Influence of muscle forces on femoral strain distribution. *Journal of Biomechanics*, 31, pp. 841-846.

Dufresne, C.L. (1797) Sur une nouvelle espèce de signe *Simia entellus. Bulletin des Sciences par la Societe Philomatique Paris*, 1, pp.49.

Erickson, G.M.; Catanese III, J.; Keaveny, T.M. (2002) Evolution of the biomechanical material properties of the femur. *The Anatomical Record*, 268, pp. 115-124.

Eriksen, E.F. (1986) Normal and pathological remodeling of human trabecular bone: Three dimensional reconstruction of the remodeling sequence in normals and in metabolic bone disease. *Endocrine Reviews*, 7[4], pp. 379-408.

Eschscholtz, J.F. (1821) *in: Entdeckungs-Reise in die Süd-See und nach der Berings-Straße zur Erforschung einer nordöstlichen Durchfahrt: unternommen in den Jahren 1815, 1816, 1817 und 1818; von Kotzebue, O. (ed.); Gebrüder Hoffmann.*

Fajardo, R.J. & Müller, R. (2001) Three-dimensional analysis of nonhuman primate trabecular architecture using micro-computed tomography. *American Journal of Physical Anthropology*, 115, pp. 327-336.

Fajardo, R.J.; Ryan, T.M.; Kappelman, J. (2002) Assessing the accuracy of high-resolution X-ray computed tomography of primate trabecular bone by comparison with histological sections. *American Journal of Physical Anthropology*, 118, pp. 1-10.

Faust, G. (2001) Charakteristika Biologischer Systeme, Fallbeispiel: Knochenumbau. *in: BIONA-report 15; Wisser, A.; Nachtigall, W. (eds.); Akademie der Wissenschaften und der Literatur*, pages 120-141.

Fischer, J. (1961) Vergleichend-anatomische Untersuchungen ber die Hft- und Oberschenkelmuskulatur von *Papio leucophaeus* (CUVIER 1807) und Mensch. *Dissertation Dsseldorf*, pages 1-67.

Fischer, K.J.; Jacobs, C.R.; Carter, D.R. (1995) Computational method for determination of bone and joint loads using bone density distributions. *Journal of Biomechanics*, 28[9], pp. 1127-1135.

Fleagle, J.G. (1976) Locomotion and posture of the malayan Siamang and implications for hominoid evolution. *Folia Primatologica*, 26, pp. 245-269.

Fleagle, J.G. (1978) Locomotion, posture, and habitat utilization in two sympatric malaysian leaf-monkeys (*Presbytis obscura* and *Presbytis melalophos*). *in: The Ecology of Arboreal Folivores; Smithsonian Institution Press*, pages 243-251.

Fleagle, J.G. (1980) Locomotion and posture. *in: Malayan Forest Primates; Chivers, D.J. (ed.); Plenum Press*, pages 191-207.

Fleagle, J.G. (1983) Locomotor adaptations of Oligocene and Miocene hominoids and their phyletic implications. *in: New Interpretations of Ape and Human Ancestry; Ciochon, R.L.; Corruccini, R.S. (eds.); Plenum Press*, pages 301-324.

Fleagle, J.G. (1988) Primate adaptation & evolution. *Academic Press*, pages 1-486.

Franzen, J.L. (2000) Auf dem Grunde des Urrheins - Ausgrabungen bei Eppelsheim. *Natur und Museum*, 130[6], pp. 169-180.

Franzen, J.L. (2002) Versuch einer Rekonstruktion der Entwicklung des rheinischen Flußsystems. *Natur und Museum*, 132[11], pp. 408-423.

Franzen, J.L.; Fejfar, O.; Storch, G. (2003a) First micromammals (mammalia, Soricomorpha) from the Vallesian (Miocene) of Eppelsheim, Rheinhessen (Germany). *Senckenbergiana lethaea*, 83[1/2], pp. 95-102.

Franzen, J.L.; Fejfar, O.; Storch, G.; Wilde, V. (2003b) Eppelsheim 2000 - new discoveries at a classical locality. *Deinsea*, 10, pp. 217-234.

Frost, H.M. (1988) Vital biomechanics: Proposed general concepts for skeletal adaptations to mechanical usage. *Calcified Tissue International*, [42], pp. 145-156.

Frost, H.M. (1990a) Skeletal structural adaptations to mechanical usage (SATMU): 1. Redefining Wolff's law: The bone modeling problem. *The Anatomical Record*, 226, pp. 403-413.

Frost, H.M. (1990b) Skeletal structural adaptations to mechanical usage (SATMU): 2. Redefining Wolff's law: The remodeling problem. *The Anatomical Record*, 226, pp. 414-422.

Frost, H.M.; Ferretti, J.L.; Jee, W.S.S. (1998) Perspectives: Some roles of mechanical usage, muscle strength, and the mechanostat in skeletal physiology, disease, and research. *Calcified Tissue International*, 62, pp. 1-7.

Fyhrie, D.P. & Carter, D.R. (1986) A unifying principle relating stress to trabecular bone morphology. *Journal of Orthopedic Research*, [4], pp. 304-317.

Gerhartz, M. (1962) Vergleichend-anatomische und vergleichend-funktionelle Untersuchung an der Hft- und Oberschenkelmuskulatur des amerikanischen Greifschwanzaffens *Ateles*. *Dissertation Dsseldorf*, pages 1-52.

Geoffroy Saint-Hilare, E. (1812) Tableau des quadrates, 1. Ord. Quadrumanes. *Annales Muséum National D'Histoire Naturelle Paris*, 19, pp. 85-122.

Gervais, P. (1849) Zoologie et Paléontologie française. ed. I, *Bertrand*.

Gieseler, W. (1926) Zur Beurteilung des Eppelsheimer Femurs. *Verhandlungen der Gesellschaft für Physische Anthropologie*, pages 34-45.

Grand, T.I. (1968a) Functional anatomy of the upper limb, chapter IX, in: Biology of the howler monkey (*Alouatta caraya*). *Bibliotheca primatologica*, 7, pp. 104-125.

Grand, T.I. (1968b) The functional anatomy of the lower limb of the Howler Monkey (*Alouatta caraya*). *American Journal of Physical Anthropology*, 28, pp. 163-182.

Gray, J.E. (1821) On the natural arrangement of vertebrose animals. *London Repository, Monthly Journal and Review*, 15, pp. 296-310.

Gray, J.E. (1825) Outline of an attempt at the disposition of the Mammalia into tribes and families with a list of the genera apparently appertaining to each tribe. *Annals of Philosophy*, n.s. 10, pp. 337-344.

Gregory, W.K. (1920) On the structure and relations of *Notharctus*, an american Eocene primate. *Memoirs of the American Museum Of Natural History*, III[II], pp. 51-241.

Groves, C.P. (1975) Systematics and Phylogeny of Gibbons. *Gibbon and Siamang*, 1, pp. 1-89.

Goldstein, S.A. (1987) The mechanical properties of trabecular bone dependence on anatomic location and function. *Journal of Biomechanics*, 20[11/12], pp. 1055-1061.

Goldstein, S.A. ; Matthews, L.S.; Kuhn, J.L.; Hollister, S.J. (1991) Trabecular bone remodeling: an experimental model. *Journal of Biomechanics*, 24[Suppl. 1], pp. 135-150.

Goulet, R.W.; Goldstein, S.A.; Ciarelli, M.J.; Kuhn, J.L.; Brown, M.B.; Feldkamp, L.A. (1994) The relationship between the structural and orthogonal compressive properties of trabecular bone. *Journal of Biomechanics*, 27[4], pp. 375-389.

Günther, M.M. (1989) Funktionsmorphologische Untersuchungen zum Sprungverhalten an mehreren Halbaffenarten. *Inaugural-Dissertation im Fachbereich Biologie der Freien Universität Berlin*, pages 1-183.

Guldberg, R.E. & Hollister, S.J. (1995) Influence of loading on the tissue modulus of trabecular bone: a combined experimental and microstructural modeling approach. *Advances in Bioengineering ASME*, BED-Vol. 31, pp. 157-158.

Guldberg, R.E.; Caldwell, N.J.; Guo, X.E.; Goulet, R.W.; Hollister, S.J.; Goldstein, S.A. (1997a) Mechanical stimulation of tissue repair in the hydraulic bone chamber. *Journal of Bone and Mineral Research*, 12[8], pp. 1295-1302.

Guldberg, R.E.; Richards, M.; Caldwell, N.J.; Kuelske, C.L.; Goldstein, S.A. (1997b) Trabecular bone adaptation to variations in porous-coated implant topology. *Journal of Biomechanics*, 30[2], pp. 147-153.

Guldberg, R.E.; Hollister, S.J.; Charras, G.T. (1998) The accuracy of digital image-based finite element models. *Journal of Biomechanical Engineering*, 120, pp. 289-295.

Hall, K.R.L. (1962) Numerical data, maintenance activities and locomotion of the wild Chamca Baboon, *Papio ursinus. Proceedings of the Zoological Society London*, 139, pp. 181-220.

Hayes, W.C. (1986) Bone mechanics: From tissue mechanical properties to an assessment of structural behavior. *in: Frontiers in Biomechanics; Schmid-Schönbein, G.W.; Woo, S.L.Y.; Zweifach, B.W. (eds.), Springer Verlag*, pages 196-209.

Heller, M.; Bergmann, G.; Deuretzbacher, G.; Claes, L.; Haas, N.P.; Duda, G.N. (2001a) Influence of femoral anteversion on proximal femoral loading: measurement and simulation in four patients. *Clinical Biomechanics*, 16, pp. 644-649.

Heller, M.O.; Bergmann, G.; Deuretzbacher, G.; Dürselen, L.; Pohl, M.; Claes, L.; Haas, N.P.; Duda, G.N. (2001b) Musculo-skeletal loading conditions at the hip during walking and stair climbing. *Journal of Biomechanics*, 34[7], pp. 883-893.

Hildebrand, T. & Rüegsegger, P. (1997a) A new method for the model-independent assessment of thickness in the three-dimensional images. *Journal of Microscopy*, 185[1], pp. 67-75.

Hildebrand, T. & Rüegsegger, P. (1997b) Quantification of bone microarchitecture with the structure model index. *Computer Methods in Biomechanics and Biomedical Engineering*, 1, pp. 15-23.

Hodge, W.A.; Carlson, K.L.; Fijan, R.S.; Burgess, R.G; Riley, P.O.; Harris, W.H.; Mann, R.W. (1989) Contact pressure from an instrumented hip endoprothesis. *The Journal of Bone and Joint Surgery*, 71-A[9], pp. 1378-1286.

Hollister, S.J. & Kikuchi, N. (1994) Homogenization theory and digital imaging: A basis for studying the mechanics and design principles of bone tissue. *Biotechnology and Bioengineering*, 43, pp. 586-596.

Huiskes, R. (1997) Simulation of self-organization and functional adaptation in bone. *Der Unfallchirurg*, (261), pp. 299-320.

Huiskes, R.; Ruimerman, R.; van Lenthe, G.H.; Janssen, J.D. (2000) Effects of mechanical forces on maintenance and adaptation of form in trabecular bone. *Nature*, 405, pp. 704-706.

Illiger, C. (1811) Prodomus systematis mammalium et avium : add. terminis zoographicis utriusque classis, eorumque versione Germanica. *Salfeld*, pages 1-301.

Ishida, H.; Kumakura, H.; Kondo, S. (1985) Primate bipedlism and quadrupedalism: Comparative electromyography. *in: Primate Morphophysiology, Locomotor Analyses and Human Bipedalism; Kondo, S. (ed.); University of Tokyo Press*, pages 59-79.

Jaasma, M.J.; Byraktar, H.H.; Niebur, G.L.; Keaveny, T.M. (2002) Biomechanical effects of intraspecimen variations in tissue modulus for trabecular bone. *Journal of Biomechanics*, 35, pp. 237-246.

Jablonski, N.G. & Chaplin, G. (1993) Origin of habitual terrestrial bipedalism in the ancestor of the hominidae. *Journal of Human Evolution*, 24, pp. 259-280.

Jensen, K.S.; Mosekilde, L.; Mosekilde, L. (1990) A model of vertebral trabecular bone architecture and its mechanical properties. *Bone*, [11], pp. 417-423.

Jensen, R.H. & Davy, D.T. (1975) An investigation of muscle lines of action about the hip: A centroid line approach vs the straight line approach. *Journal of Biomechanics*, 8, pp. 103-110.

Kasra, M. & Grynpas, M.D. (1998) Static and dynamic finite element analyses of an idealized structural model of vertebral trabecular bone. *Journal of Biomechanical Engineering*, 120, pp. 267-272.

Keaveny, T.M. Strength of trabecular bone. *in: Bone Mechanics Handbook 2. Ed.; Cowin, S.C. (ed.); CRC Press*, pages 16-1 - 16-42.

Keaveny, T.M. & Hayes, W.C. (1993) Mechanical properties of cortical and trabecular bone. *in: Bone, Volume 7: Bone Growth - B, chapter 10; Hall, B.K. (ed.); CRC Press*, pages 285-345.

Keaveny, T.M.; Borchers, R.E.; Gibson, L.J.; Hayes, W.C. (1993) Trabecular bone modulus and strength can depend on specimen geometry. *Journal of Biomechanics*, 26[8], pp. 991-1000.

Keaveny, T.M.; Morgan, E.F.; Niebur, G.L.; Yeh, O.C. (2001) Biomechanics of trabecular bone. *Annual Review of Biomedical Engineering*, 3, pp. 307-333.

Keyak, J.H. & Rossi, S.A. (2000) Prediction of femoral fracture load using finite element models: An examination of stress- and strain-based failure theories. *Journal of Biomechanics*, 33, pp. 209-214.

Kimura, T. (1985) Bipedal and quadrupedal walking of primates: Comparative dynamics. *in: Primate Morphophysiology, Locomotor Analyses and Human Bipedalism; Kondo, S. (ed.); University of Tokyo Press*, pages 81-104.

Kleerkoper, M.; Villanueva, A.R.; Stanciu, J.; Sudhaker Rao, D.; Parfitt, A.M. (1985) The role of three-dimensional trabecular microstructure in the pathogenesis of vertebral compression fractures. *Calcified Tissue International*, [37], pp. 594-597.

Kolar, K. (1988) Lemuren. *in: Grzimeks Enzyklopädie der Säugetiere, Vol. 2; Grzimek, B. (ed.); Kindler Verlag*, pages 42-76.

Kothari, M.; Keaveny, T.M.; Lin, J.C.; Newitt, D.C; Genant, H.K.; Majumdar, S. (1998) Impact of spatial resolution on the prediction of trabecular architecture parameters. *Bone*, 22[5], pp. 437-443.

Kotzar, G.M.; Cavy, D.T.; Goldberg, V.M.; Heiple, K.G.; Berilla, J.; Heiple jr., K.G.; Brown, R.H.; Burstein, A.H. (1991) Telemeterized in vivo hip joint force data:

A report on two patients after total hip surgery. *Journal of Orthopaedic Research*, 9, pp. 621-633.

Krieg, H. (1928) Schwarze Brüllaffen (*Alouatta caraya* Humboldt). Tagebuch-Aufzeichnungen auf der Deutschen Chaco-Expedition. *Zeitschrift für Säugetrierkunde*, II, pp. 119-132.

Kummer, B. (1959) Bauprinzipien des Säugerskeletes. *Thieme Verlag*, pages 1-235.

Lacépède, B.G.R. (1799) Tableau des division sousdivisions, ordres et generas des mammifères. *in: Histoire Naturelle; de Buffon, Vol. 14; G.L.F. (ed.); P. Didot LÁine et Firmin Dido*, pages 144-195.

Laib, A.; Barou, O.; Vico, L.; Lafage-Proust, M.H.; Alexandre, C. Rügsegger, P. (2000) 3D micro-computed tomography of trabecular and cortical bone architecture with application to a rat model of immobilisation osteoporosis. *Medical and Biological Engineering and Computing*, 38, pp. 326-332.

Lakes, R. (2001) Viscoelastic properties of cortical bone. *in: Bone Mechanics Handbook 2. Ed.; Cowin, S.C. (ed.); CRC Press*, pages 11-1 - 11-15.

Lakes, R.S. & Katz, J.L. (1979) Viscoelastic properties of wet cortical bone - II. Relaxation mechanisms. *Journal of Biomechanics*, 12, pp. 679-687.

Langdon, J.H. (1986) Functional morphology of the Miocene hominoid foot. *Contributions to Primatology*, 22, pp. 1-225.

Lanyon, L.E. (1974) Experimental support for the trajectorial theory of bone structure. *The Journal of Bone and Joint Surgery*, 56 B[1], pp. 160-166.

Lanyon, L.E. (1981) Locomotor loading and functional adaptation in limb bones. *Symposia of the Zoological Society of London*, 48, pp. 305-329.

Lanyon, L.E. (1982) Mechanical function and bone remodeling. *in: Bone in Clinical Orthopaedics; Sumner-Smith, G. (ed.); W.B. Saunders Company*, pages 273-304.

Lanyon, L.E. & Rubin, C.T. (1985) Functional adaptation in skeletal structures. *in: Functional Vertebrate Morphology; Hildebrand, M.; Bramble, D.M.; Liem, K.F.; Wake, D.B. (eds.); Belknap Press*, pages 1-25.

Lartet, E. (1856) Note sur un grand Singe fossile qui se rattache au groupe des Singes supérieurs. *Extrait des Comptes rendus des séances de l'Académie des Sciences*, 43, pp. 219-223.

Le Gros Clark, W.E. & Leaky, L.S.B. (1951) The Miocene hominoidean of east africa. *British Museum (Natural History) Fossil Mammals of Africa*, [1], pp. 1-117.

Lieberman, D.E.; Devlin, M.J.; Pearson, O.M. (2001) Articular area responses to mechanical loading: Effects of exercise, age, and skeletal location. *American Journal of Physical Anthropology*, 116, pp. 266-277.

Linnaeus, C. (1758) Systema naturae per regna tria naturae, secundum calsses, ordines genera, species cum characteribus, differentris, synonymis, locis. Editis decima, reformata. *Laurentii Salvii*, pages 1-823.

Linnaeus, C. (1766) Systema naturae per regna tria naturae, secundum calsses, ordines genera, species cum characteribus, differentris, synonymis, locis. 12th ed. *Laurentii Salvii*, pages 1-532.

Linnaeus, C. (1771) Mantissa Plantarum. *Laurentii Salvii*.

Linde, F.; Norgaard, P.; Hvid, I.; Odgaard, A.; Soballe, K. (1991) Mechanical properties of trabecular bone. Dependency on strain rate. *Journal of Biomechanics*, 24[9], pp. 803-809.

Lovejoy, C.O. (1984) Die Evolution des aufrechten Ganges. *Verständliche Forschung, Evolution des Menschen, Spektrum der Wissenschaft*, pages 58-66.

Macchiarelli, R.; Bondioli, L.; Galichon V.; Tobias, P.V. (1999) Hip bone trabecular architecture shows uniquely distinctive locomotor behaviour in south african australopithecines. *Journal of Human Evolution*, [36], pp. 211-232.

MacLatchy, L. & Müller, R. (2002) A comparison of the femoral head and neck trabecular architecture of Galago and Perodictius using micro-computed tomography (μCT). *Journal of Human Evolution*, 43, pp. 89-105.

Marchal, F. (2000) A new morphometric analysis of the hominid pelvic bone. *Journal of Human Evolution*, 38, pp. 347-365.

Martill, D.M. (1991) Bones as stones: the contribution of vertebrate remains to the lithologic record. *The Process of Fossilization; Donovan, S.K. (ed.)*, pages 270-292.

Martin, R.D. (1990) Primate origins and evolution. *Chapman & Hall*, pages 1-804.

McHenry, H. & Corruccini, R.S. (1976) Affinities of tertiary hominoid femora. *Folia Primatologica*, 26, pp. 139-150.

McNeill Alexander, R. (1985) Body support, scaling, and allometry. *in: Functional Vertebrate Morphology; Hildebrand, M.; Bramble, D.M.; Liem, K.F.; Wake, D.B. (eds.); Belknap Press*, pages 26-37.

McPhearson, A. & Juhasz, L. (1965) The haemodynamics of bone. *in: Biomechanics and related bio-engineering topics; Kenedi, R.M. (ed.); Pergamon Press*, pages 181-186.

Mein, P. (1986) Chronological succsession of hominoids in the european neogene. *in: Primate Evolution; Else, J.G.; Lee, P.C. (eds.); Cambridge University Press*, pages 59-70.

Menschen und Tiere - Bei den Pavianen. by Borland, R. *ORF*.

Morgan, E.F. & Keaveny, T.M. (2001) Dependence of yield strain of human trabecular bone on anatomic site. *Journal of Biomechanics*, 34, pp. 569-577.

Morgan, E.F.; Bayraktar, H.H.; Yeh, O.C.; Keaveny, T.M. (2002) Contribution of inter-site differences in architecture to trabecular bone yield behavior. *Transactions Orthopaedic Research Society*, page 121.

Mosekilde, L. (1990) Consequences of the remodelling process for vertebral trabecular bone structure: A scanning electron microscopy study (uncoupling of unloaded structures). *Bone and Mineral*, 10, pp. 13-35.

Müller, P.L.S. (1773) Des Ritters Carl von Linné Königlich Schwedischen Leibarztes etc. etc. vollstaendiges Natursystem: nach der zwoelften lateinischen Ausgabe und nach Anleitung des hollaendischen Houttuynischen Werks mit einer ausfuehrlichen Erklaerung / ausgefertiget von Philipp Ludwig Statius Müller. Vol. 1, *G. N. Raspe*, pages 1-508.

Müller, R.; Van Campenhout, H.; Van Damme, B.; Van der Perre, G.; Dequeker, J.; Hildebrand, T.; Rüegsegger, P. (1998) Morphometric analysis of human bone biopsies: A quantitative structural comparison of histological sections and micro-computed tomography. *Bone*, 23, pp. 59-66.

Mullender, M.G.; Huiskes, R.; Weinans, H. (1994) A physiological approach to the simulation of bone remodeling as a self-organizational control process. *Journal of Biomechanics*, 27[11], pp. 1389-1394.

Mullender, M.G. & Huiskes, R. (1995) Proposal for the regulatory mechanism of Wolff's law. *Journal of Orthopaedic Research*, 13[4], pp. 503-512.

Mullender, M.G; Huiskes, R.; Versleyen, H.; Buma, P. (1996) Osteocyte density and histomorphometric parameters in cancellous bone of the proximal femur in five mammalian species. *Journal of Orthopaedic Research*, 14, pp. 972-979.

Napier, J.R. (1976) Primate locomotion. *Oxford Biology Readers*, 41, pp. 3-16.

Neckles, R. (2004) Red howler monkey. *http://www.glwildlife.org/glwildlife/neckles.html, published with permission.*

Newitt, D.C.; Majumdar, S. van Rietbergen, B.; von Ingersleben, G.; Harris, S.T.; Genant, H.K.; Chesnut, C.; Garnero, P.; McDonald, B. (2002) In vivo assessment of architecture and micro-finite element analysis derived indices of mechanical properties of trabecular bone in the radius. *Osteoporosis International*, 13, pp. 6-17.

Niebur, G.L.; Feldstein, M.J.; Yuen, J.C.; Chen, T.J.; Keaveny, T.M. (2000) High-resolution finite element models with tissue strength asymmetry accurately predict failure of trabecular bone. *Journal of Biomechanics*, 33, pp. 1575-1583.

Nikolei, J. (2002) Lokomotionsökologie adulter Hanuman Languren (*Semnopithecus entellus*) in einem saisonalen Waldhabitat in Ramnagar, Südnepal. *Inaugural-Dissertation im Fachbereich Biologie der Freien Universität Berlin*, pages 1-297.

Nowak, R.M. (1991) Walker's mammals of the world, Vol. 1. *The Johns University Press*, pages 1-642.

Ochoa, J.A.; Sanders, A.P.; Heck, D.A.; Hillberry, B.M. (1991) Stiffening of the femoral head due to intertrabecular fluid and intraosseous pressure. *Journal of Biomechanical Engineering*, 113, pp. 259-262.

Odgaard, A. & Linde, F. (1991) The underestimation of young's modulus in compressive testing of cancellous bone specimens. *Journal of Biomechanics*, 24[8], pp. 691-698.

Odgaard, A. & Gundersen, H.J.G. (1993) Quantification of connectivity in cancellous bone, with special emphasis on 3-d reconstructions. *Bone*, 14, pp. 173-182.

Okada, M. (1985) Primate bipedal walking: Comparative kinematics. *in: Primate Morphophysiology, Locomotor Analyses and Human Bipedalism; Kondo, S. (ed.); University of Tokyo Press*, pages 47-58.

Okada, M.; Yamazaki, N.; Ishida, H.; Kimura, T.; Kondo, S. (1983) Biomechanical characteristics of hylobatid bipedal walking on flat surfaces. *Annales des Sciences Naturelles, Zoologie*, 5, pp. 137-144.

Ott, S.M. (1996) Theoretical and methodical approach. *in: Principles of Bone Biology; Bilezikian, J.P.; Raisz, L.G.; Rodan, G.A. (eds.); Academic Press*, pages 231-241.

Parfitt, M.; Drezner, M.K.; Glorieux, F.H.; Kanis, J.A.; Malluche, H.; Meunier, P.J.; Ott, S.M.; Recker, R.P. (1987) Bone histomorphometry: Standardization of nomenclature, symbols, and units. *Journal of Bone and Mineral Research*, 2[6], pp. 595-611.

Pauwels, F. (1965) Gesammelte Abhandlungen zur funktionellen Anatomie des Bewegungsapparates. *Springer Verlag*, pages 1-543.

Pauwels, F. (1980) Biomechanics of the locomotor apparatus. *Springer Verlag*, pages 1-518.

Peyrin, F.; Salomé, M.; Cloetens, P.; Laval-Jeantet, A.M.; Ritman, E.; Rüegsegger, P. (1998) Micro-CT examinations of trabecular bone samples at different resolutions: 14, 7 and 2 micron level. *Technology and Health Care*, [6], pp. 391-401.

Peyrin, F.; Muller, C.; Carillon, Y.; Nuzzo, S.; Bonnaisse, A.; Briguet, A. (2001) Synchrotron radiation μCT: a reference tool for the characterization of bone samples. *in: Noninvasive Assessment of Trabecular Bone Architecture and the Competence of Bone; Majumdar & Bay (eds.); Kulwer Academic/Plenum Publishers*, pages 129-142.

Platzer, W.; Kahle, W.; Leonhardt, H. (1986) Taschenatlas der Anatomie. *Thieme Verlag*, pages 1-436.

Pocock, R.I. (1918) On the external characters of the lemurs and of *Tarsius*. *Proceedings of the Zoological Society London, 1918*, pp. 19-53.

Pohlig, H. (1892) "without title". *Sitzungs Bericht der Niederrheinischen Gesellschaft in Bonn; cited after Gieseler, W. (1926); Zur Beurteilung des Eppelsheimer Femurs; Verhandlungen der Gesellschaft für Physische Anthropologie, p. 34-45*; pp. 41-43.

Pohlig, H. (1895) Paidopithex rhenanus, n.g.n.dp., le Signe anthropomotphe du Pliocène rhénan. *Bulletin de la Société Belge de Géologie*, IX, pp. 149-151.

Preuschoft, H. (1988) Kleine Menschenaffen oder Gibbons. *in: Grzimeks Enzyklopädie der Säugetiere, Vol. 2; Grzimek, B. (ed.); Kindler Verlag*, pages 328-356.

Preuschoft, H. & Witte, H. (1993) Die Körpergestalt des Menschen als Ergebnis biomechanischer Erfordernisse. *in: Evolution und Anpassung. Warum die Vergangenheit die Gegenwart erklärt. Christian Vogel zum 60. Geburtstag; Voland, E. (ed.); S. Hirzel Verlag*, pages 43-74.

Priemel, G. (1937) Die platyrrhinen Affen als Bewegungstypen. *Zeitschrift für Morphologie und Ökologie der Tiere, Inaugural-Dissertation der philosophischen Fakultät II. Sektion der Ludwig-Maximilians-Universität München*, 33(1), pp. 1-53.

Prost, J.H. (1967) Bipedalism of man and gibbon compared using estimates of joint motion. *American Journal of Physical Anthropology*, 26, pp. 135-148.

Prost, J.H. (1980) Origin of bipedalism. *American Journal of Physical Anthropology*, 52, pp. 175-189.

Raffles, T.S. (1821) Second part of the descriptive catalogue of a zoological collection, made on account of the honourable East India Company, in the island of Sumatra and its vicinity. *Transactions of the Linnean Society of London*, 13, pp. 277-340.

Rafferty, K.L. (1998) Structural design of the femoral neck in primates. *Journal of Human Evolution*, 34[4], pp. 361-383.

Rice, J.C.; Cowin, S.C.; Bowman, J.A. (1988) On the dependence of the elasticity and strength of cancellous bone on apparent density. *Journal of Biomechanics*, 21[2], pp. 155-168.

Rook, L.; Bondioli, L.; Köhler, M.; Moyà-Solà, S.; Macchiarelli, R. (1999) Oreopithecus was a bipedal ape after all: Evidence from the iliac cancellous architecture. *Proceedings of the National Academy of Sciences*, 96, pp. 8795-8799.

Rose, M.D. (1994) Quadrupedalism in some Miocene catarrhines. *Journal of Human Evolution*, 26[5/6], pp. 387-411.

Rubin, C.T.; McLeod, K.J.; Bain; S.D. (1990) Functional strains and cortical bone adaptation: epigenetic assurance of skeletal integrity. *Journal of Biomechanics*, 23[Suppl. 1], pp. 43-54.

Rüegsegger, P.; Koller, B.; Müller, R. (1996) A microtomographic system for the nondestructive evaluation of bone architecture. *Calcified Tissue International*, [58], pp. 24-29.

Ruff, C. (1988) Hindlimb articular surface allometry in hominoidea and *Macaca*, with comparison to diaphyseal scaling. *Journal of Human Evolution*, 17, pp. 687-714.

Ryan, T.M. & Ketcham, R.A. (2002a) Femoral head trabecular bone structure in two omomyid primates. *Journal of Human Evolution*, 42, pp. 241-263.

Ryan, T.M. & Ketcham, R.A. (2002b) The three-dimensional structure of trabecular bone in the femoral head of strepsirrhine primates. *Journal of Human Evolution*, 43, pp. 1-26.

Ryan, T.M. & van Rietbergen, B. (2004) Mechanical significance of femoral head trabecular bone structure in *Loris* and *Galago* evaluated using micromechanical finite element models. *American Journal of Physical Anthropology, Early View*, 1-13, DOI 10.1002/ajpa.10414

Salamone, L.M.; Glynn, N.; Black, D.; Epstein, R.S.; Palermo, L.; Meilahn, E.; Kuller, L.H.; Cauley, J.A. (1995) Body composition and bone mineral density in premenopausal and early perimenopausal women. *Journal of Bone and Mineral Research*, 10[11], pp. 1762-1768.

Salomé, M.; Peyrin, F.; Cloetens, P.; Odet, C.; Laval-Jeantet, A.-M. (1999) A synchrotron radiation microtomography system for the analysis of trabecular bone samples. *Medical Physics*, 26[10], pp. 2194-2204.

Scanco (2005a) *http* : *//www.scanco.ch.*

Scanco (2005b) *http* : *//www.scanco.ch/download/uct*40_*manual.pdf*.

Schaffler, M.B. & Burr, D.B. (1984) Primate cortical bone microstructure: Relationship to locomotion. *American Journal of Physical Anthropology*, 65, pp. 191-197.

Scherf, H (2000) Funktionelle Bedeutung der femoralen Konstruktion bei ausgewählten Primaten und Insektivoren. *Diploma Thesis, TU Darmstadt*, pages 1-99.

Scherf, H.; Beckmann, F.; Fischer, J.; Witte, F. (2004) Internal channel structures in trabecular bone. *Optical Science and Technology SPIE's 49th Annual Meeting, Proceedings of SPIE*, Vol. 5535 - Developments in X-Ray Tomography IV, Ulrich Bonse, ed., pp. 792-798.

Scherf, H.; Koller, B.; Schrenk, F. (2005) Locomotion related structures in the femoral trabecular architecture of Primates and Insectivores. *Senckenbergiana biologica*, 85[1], pp. 101-112.

Schönau, E. (1998) The development of the skeletal system in children and the influence of muscular strength. *Hormone Research*, 49, pp. 27-31.

Simon, M.; Sauerwein, C.; Tiseanu, I.; Burdairon, S. (2001) 3D Flexible Computertomographie mit RayScan 200. *DGZfP-Jahrestagung 2001 - Zerstörungsfreie Materialprüfung, 21.-23. Mai Berlin, Berichtsband 75-CD*, pp. 1-7.

Simons, E.L. & Pilbeam, D.R. (1965) Preliminary revision of the Dryopithecinae (Pongidae, Anthropoidea). *Folia Primatologica*, 3[2-3], pp. 81-152.

Simons, E.L. & Fleagle, J. (1973) The history of extinct gibbon-like primates. *Gibbon and Siamang*, 2, pp. 121-148.

Soderberg, G.L. & Dostal, W.F. (1978) Electromyographic study of three parts of the gluteus medius muscle during functional activities. *Physical Therapy*, 58[6], pp. 691-696.

Steininger, F.F. (1999) Chronostratigraphy, geochronology and biochronology of the Miocene "European Land Mammal Mega-Zones" (ELMMZ) and the Miocene "Mammal-Zones (MN-Zones)". *in: Land Mammals of Europe; Rössner, G.E.; Heissig, K. (eds.); Verlag Dr. Friedrich Pfeil*, pages 9-24.

Stenström, M.; Olander, B.; Letho-Axelius, D.; Madsen, J.E.; Nordsletten, L.; Carlsson, G.A. (2000) Bone mineral density and bone structure parameters as predictors of bone strength: as analysis using computerized microtomography and gastrectomy-induced osteopenia in the rat. *Journal of Biomechanics*, [33], pp. 289-297.

Stülpner, M.A.; Reddy, B.D.; Starke, G.R.; Spirakis, A. (1997) A three-dimensional finite analysis of adaptive remodelling in the proximal femur. *Journal of Biomechanics*, 30[10], pp. 1063-1066.

Swanson, S.A.V. & Freeman, M.A.R. (1966) Is bone hydraulically strengthened?. *Medical and Biological Engineering*, 4, pp. 433-438.

Swartz, S.M.; Parker, A.; Huo, C. (1998) Theoretical and empirical scaling patterns and topological homology in bone trabeculae. *The Journal of Experimental Biology*, 201, pp. 573-590.

Szalay, F.S. & Delson, E. (1979) Evolutionary history of the primates. *Academic Press*, pages 1-580.

Thompson, J.B.; Kindt, J.H.; Drake, B.; Hansma, H.G.; Morse, D.E.; Hansma, P.K. (2001) Bone indentation recovery time correlates with bond reforming time. *Nature*, 414, pp. 773-776.

Tsubota, K.; Adachi, T.; Tomita, Y. (2002) Functional adaptation of cancellous bone in human proximal femur predicted by trabecular surface remodeling simulation toward uniform stress state. *Journal of Biomechanics*, 35, pp. 1541-1551.

Turner, C.H. (1992) On Wolff's law of trabecular architecture. *Journal of Biomechanics*, 25[1], pp. 1-9.

Turner, C.H.; Cowin, S.C.; Rho, J.Y.; Ashman, R.B.; Rice, J.C. (1990) The fabric dependence of the orthotropic elastic constants of cancellous bone. *Journal of Biomechanics*, 23[6], pp. 549-561.

Turner, C.H. & Burr, D.B. (1993) Basic biomechanical measurements of bone: A tutorial. *Bone*, 14, pp. 595-606.

van Hooff, J.A.R.A.M. (1988) Meerkatzenartige. *in: Grzimeks Enzyklopädie der Säugetiere, Vol. 2; Grzimek, B. (ed.); Kindler Verlag*, pages 208-285.

van Lenthe, G.H. & Huiskes, R. (2002) How morphology predict mechanical properties of trabecular structures depends on intra-specimen trabecular thickness variations. *Journal of Biomechanics*, 35, pp. 1191-1197.

van der Linden, J.C.; Birkenhäger-Frenkel, D.H.; Verhaar, J.A.N.; Weinans, H. (2001) Trabecular bone's mechanical properties are affected by its non-uniform mineral distribution. *Journal of Biomechanics*, 34, pp. 1573-1580.

van Rietbergen, B.; Huiskes, R.; Eckstein, F.; Rüegsegger, P. (2003) Trabecular bone tissue strains in the healthy and osteoporotic human femur. *Journal of Bone and Mineral research*, 18[10], pp. 1781-1788.

Vereecke, E. (2006) The functional morphology and bipedal locomotion of Hylobates lar: and its implications for the evolution of hominin bipedalism.- Antwerpen: Universiteit Antwerpen, Faculteit Wetenschappen, Departement Biologie - Doctoraal proefschrift, pages 1 - 308

Vogel, C. & Winkler, P. (1988) Schlank- und Stummelaffen. *in: Grzimeks Enzyklopädie der Säugetiere, Vol. 2; Grzimek, B. (ed.); Kindler Verlag*, pages 296-325.

Vogel, M.; Hahn, M.; Pompesius-Kempa, N.; Delling, G. (1989) Trabucular microarchitecture of the human spine. *Neuere Ergebnisse in der Osteologie; Jahrestagung der Deutschen Gesellschaft für Osteologie, 4; Springer, Berlin*, pages 449-455.

Walkhoff, O. (1904) Das Femur des Menschen und der Anthropomorphen in seiner funktionellen Gestalt. *Studien über die Entwicklungsmechanik des Primatenskeletts*, 1, pages 1-58.

Weaver, J.K. & Chalmers, J. (1966) Cancellous bone: Its strength and changes with aging and an evaluation of some method for measuring its mineral content. *The Journal of Bone and Joint Surgery*, 48-A[2], pp. 289-298.

Welker, C. & Schäfer-Witt, C. (1988) Kapuzinerartige. *in: Grzimeks Enzyklopädie der Säugetiere, Vol. 2; Grzimek, B. (ed.); Kindler Verlag*, pages 122-177.

Welten, D.C.; Kemper, H.C.G.; Post, G.B.; van Mechelen, W.; Twisk, J.; Lips, P.; Teule, G.J. (1994) Weight-bearing activity during youth is a more important factor for peak bone mass than calcium intake. *Journal of Bone and Mineral Research*, 9[7], pp. 1089-1096.

Whalen, R.T.; Carter, D.R.; Steele, C.R. (1988) Influence of physical activity on the regulation of bone density. *Journal of Biomechanics*, 21[10], pp. 825-837.

Whitehouse, W.J. (1974) The quantitative morphology of anisotropic trabecular bone. *Journal of Microscopy*, 101[2], pp. 153-168.

Whitehouse, W.J. & Dyson, E.D.; Jackson, C.K. (1971) The scanning electron microscope in studies of trabecular bone from a human vertebral body. *Journal of Anatomy*, 108, pp. 481-496.

Whitehouse, W.J. & Dyson, E.D. (1974) Scanning electron microscope studies of trabecular bone in the proximal end of the human femur. *Journal of Anatomy*, 118[3], pp. 417-444.

Williams, J.L. & Lewis, J.L. (1982) Properties and an anisotropic model of cancellous bone from the proximal tibial epiphysis. *Journal of Biomechanical Engineering*, 104, pp. 50-56.

Wirtz, C.D.; Schiffers, N.; Pandorf, T.; Radermacher, K.; Weichert, D.; Forst, R. (2000) Critical evaluation of known bone material properties to realize anisotropic FE-simulation of the proximal femur. *Journal of Biomechanics*, 33, pp. 1325-1330.

Wolff, J. (1892) Das Gesetz der Transformation der Knochen. *August Hirschwald Verlag*, pages 1-152.

Yamazaki, N. (1985) Primate bipedal walking: Computer simulation. *in: Primate Morphophysiology, Locomotor Analyses and Human Bipedalism; Kondo, S. (ed.); University of Tokyo Press*, pages 105-130.

Zapfe, H. (1960) Die Primatenfunde aus der miozänen Spaltenfüllung von Neudorf an der March (Děvínská Nová Ves), Tschechoslowakei. *Schweizerische Palaeontologische Abhandlungen*, 78, pp. 1-293.

Zapfe, H. & Hürzeler, J. (1957) Die Fauna der miozänen Spaltenfüllung von Neudorf an der March (ČSR.). Primates. *Sitzungs-Bericht der österreichischen Akademie der Wissenschaften mathematisch-naturwissenschaftliche Klasse Abteilung I*, 166, pp. 114-123.

Zuckerman, S.; Ashton, E.H.; Flinn, R.M.; Oxnard, C.E.; Spence, T.F. (1973) Some locomotor features of the pelvic girdle in primates. *Symposia of the Zoological Society of London*, 33, pp. 71-165.

Zysset, P.K.; Guo, X.E.; Hoffler, E.; Moore, K.E.; Goldstein, S.A. (1999) Elastic modulus and hardness of cortical and trabecular bone lamellae measured by nanoindentation in the human femur. *Journal of Biomechanics*, 32, pp. 1005-1012.

Curriculum Vitae

Education

Viktoriaschule, Darmstadt (High-school)	(08/87 - 06/93)
Darmstadt University of Technology	(10/93 - 08/06)
Diploma Geology - Paleontology	(05/00)

Experience

Darmstadt University of Technology, Forschungsinstitut Senckenberg, Ph. D. Research	(01/01 - 08/06)

Refereed Publications

H. Scherf "Virtuelles 3D Modell der Fossilienfundstätte Grube Messel", *Cour. Forsch. Senck.*, 252 ,2004, pp. 233-236.

H. Scherf, F. Beckmann, J. Fischer, F. Witte "Internal channel structures in trabecular bone", Optical Science and Technology SPIE's 49th Annual Meeting, Proceedings of SPIE, Vol. 5535 - Developments in X-Ray Tomography IV, Ulrich Bonse, ed., 2004, pp. 792-798.

H. Scherf, J. Habersetzer, R. Seidel, F. Beckmann "3-D-Animation knöcherner Gesamskelette und mikro-tomographischer Fossilien aus der Grube Messel", *Cour. Forsch. Senck.*, 252, 2004, pp. 237-241.

H. Scherf, B. Koller, F. Schrenk "Locomotion related structures in the femoral trabecular architecture of Primates and Insectivores", *Senck. biol.*, 85[1], 2005, pp. 101-112.

Oral Presentations

H. Scherf, "Mikrocomputertomographische Untersuchungen der femoralen Trabekelarchitektur an verschiedenen Primaten und Insektivoren", 28. Meeting of the Arbeitskreis Wirbeltierpaläontologie, Kusel, Germany, 2001

H. Scherf, F. Schrenk "Microcomputertomographic investigation of the femoral trabecular architecture on different Primates and Insectivores", VI European Workshop on Vertebrate Paleontology, Florence, Italy, 2001

H. Scherf, F. Beckmann, J. Habersetzer "Differentiation in the mineral content of trabecular bone", 51. SVPCA Symposium, Oxford, Great Britain, 2003

H. Scherf, J. Habersetzer "High resolution CT: Entering a new dimension in palaeontology", Workshop - 3D Advances in Natural History and Cultural Heritage, Senckenberg Research Institute and Natural History Museum, Frankfurt/Main, Germany, 22.04.2005

H. Scherf, F. Beckmann, J. Habersetzer, F. Schrenk "Application of High-resolution CT-images for Investigation of the trabecular architecture of primates and Eocene Messel fossils", IX. International Mammalogical Congress, Sapporo, Japan, 2005

Poster Presentation

H. Scherf, F. Beckmann, J. Fischer, F. Witte "Internal channal structures in trabecular bone International Conference "Developments in X-Ray Tomography IV", Optical Science and Technology Symposium, SPIE's 49th Meeting, Denver 02.-06.08.2004

Zusammenfassung

Der Schwerpunkt der vorliegende Arbeit war die Untersuchung des Einflusses von lokomotorischen Belastungen auf die Spongiosaarchitektur des proximalen Femurs bei verschiedenen Primaten. Fünf rezente Arten dienten als Vergleichsbasis für die Analyse der Spongiosaarchitektur der beiden miozänen Spezies *Pliopithecus vindobonensis* und *Paidopithex rhenanus* hinsichtlich deren bevorzugter Fortbewegungsweise. Diese Arbeit basiert auf der bereits im 19. Jahrhundert erlangten Erkenntnis, daß sich Knochen Belastungszuständen aktiv anpassen kann (Wolff 1892). Zudem wird davon ausgegangen, dass spezifische habituelle Bewegungsweisen spezifische Belastungen am und im Femur hervorrufen. Diese Lastfälle stehen in direktem Zusammenhang mit dem Körpergewicht und der Muskelaktivität (Pauwels 1965, Duda 1996) und werden durch die verschiedenen Positionen des Körperschwerpunktes während der Bewegung und der Muskeln die an dem Bewegungsvorgang beteiligt sind hervorgerufen. Aufgrund dieser lokomotionsbedingten Belastungszustände des Femurs und der Anpassungsfähigkeit von Knochen an spezifische Belastungen wird davon ausgegangen, daß anhand der Spongiosaarchitektur verschiedene habituelle Fortbewegungsweisen unterschieden werden können.

Die Untersuchungen erfolgten an dreidimensionalen Darstellungen der Spongiosaarchitektur, die durch hochauflösenden Computertomographie (CT) gewonnen wurden. Anhand dieser 3D-Aufnahmen wurde die proximale femorale Spongiosaarchitektur beschrieben und im Bereich des Trochanter minor histomorphometrisch analysiert und somit quantifiziert. Anhand von 3D CT Aufnahmen wurden FEM (Finite Element Methode) Modelle erstellt. In nachfolgenden FE Analysen wurden lokomotorische Belastungen an diesen Modelle simuliert und die Vorraussetzungen für korrekte FE Analysen der Spongiosa konkretisiert. Die Ergebnisse der histomorphometrischen Analyse und der Beschreibung der Spongiosaarchitekturen der rezenten Arten erlaubten eine modellhafte Charakterisierung der verschiedenen Fortbewegungsweisen anhand der Spongiosa. Die entsprechenden Ergebnisse der fossilen Spezies wurden damit verglichen und ermöglichten eine Einschätzung der lokomotorischer Präferenzen von *Pliopithecus vindobonensis* und *Paidopithex rhenanus*.

Weitergehende Untersuchungen der verschiedenen Fortbewegungsweisen und der Biomechanik des Skelettapparates können die vorgestellte Analysemethode der Spongiosaarchitektur in der Zukunft weiter verbessern. Die vorliegende Arbeit liefert neue Einblicke in die Anpassung von spongider Knochensubstanz an verschiedene Belastungszustände und kann als Basis für weitere

Untersuchungen genutzt werden kann. Spongiosauntersuchungen können als Erweiterung der klassischen Methoden zur Analyse von habituellen Fortbewegungsweisen fossiler Spezies wertvolle Hinweise liefern. Hiermit kann insbesondere die Interpretation bei fossilen Einzelfunden erleichtert werden.

Eidesstattliche Erklärung

Hiermit erkläre ich an Eides statt, dass ich meine Dissertation selbstständig und nur mit den angegebenen Hilfsmitteln angefertigt habe. Ich habe zu keinem früheren Zeitpunkt den Versuch einer Promotion unternommen.

Roßdorf, 24. Juli 2006

Heike Scherf